THE ASTROPHYSICAL JOURNAL, 417:63–81, 1993 November 1

A REEVALUATION OF THE EXCITATION MECHANISM OF LINERS

LUIS C. HO AND ALEXEI V. FILIPPENKO[1]
Department of Astronomy, University of California, Berkeley, CA 94720
AND
WALLACE L. W. SARGENT
Palomar Observatory, 105-24 Caltech, Pasadena, CA 91125
Received 1992 December 21; accepted 1993 May 10

ABSTRACT

We present high-quality spectra of a sample of 13 low-ionization nuclear emission-line regions (LINERs) observed in the range ~3400–9800 Å at ~5–8 Å resolution. Starlight removal is achieved by the subtraction of a suitable absorption-line "template" galaxy, allowing accurate measurement of emission lines. We use the line fluxes to examine several candidates for the excitation mechanism of those LINERs whose emission-line gas is largely confined to radii $\lesssim 200$ pc. We find that photoionization by a nonstellar ionizing continuum provides the best overall explanation for the spectra over the optical–to–near-infrared region. This is supported by the detection of broad Hα emission, a correlation between line width and critical density of the forbidden lines, and pointlike X-ray emission in several of these objects. Wolf-Rayet stars or unusually hot O stars are less probable photoionization sources, especially for LINERs which exhibit broad Hα emission. The prevalence of shock heating in galactic nuclei cannot be readily evaluated with the present plane-parallel shock models, although it is likely to be an important excitation mechanism for LINERs with spatially extended emission. A small fraction of objects previously classified as LINERs may be undergoing active star formation in or near their nuclei.

Subject headings: galaxies: active — galaxies: ISM — galaxies: nuclei — galaxies: Seyfert

1. INTRODUCTION

Classical active galactic nuclei (AGNs) are rare, comprising less than 1% of luminous galaxies (Weedman 1977). In the past decade, however, spectroscopic surveys of nearby galaxies have shown that nuclear "activity" in galaxies may be much more common than previously thought (Heckman 1980, hereafter H80; Stauffer 1982; Keel 1983a, b; Filippenko & Sargent 1985; Véron-Cetty & Véron 1986; Phillips et al. 1986). These surveys indicate that as many as 10%–20% of bright, nearby galaxies may be active, but with the level of activity being much smaller than that in classical AGNs. By far the most common low-luminosity AGNs are low-ionization nuclear emission-line regions (LINERs; H80), which may comprise up to 80% of Sa, 40% of Sb, and one-third of all spiral galaxies.

The optical spectra of LINERs are characterized by strong low-ionization emission lines. According to H80's definition, LINERs have [O II] $\lambda 3727 \gtrsim$ [O III] $\lambda 5007$ and [O I] $\lambda 6300 \gtrsim (\frac{1}{3})$ [O III] $\lambda 5007$.[2] Often, [N II] $\lambda 6583/\mathrm{H}\alpha$[3] is high ($\gtrsim 0.6$) among prototypical LINERs. Because [N II] $\lambda 6583$ and Hα are close in wavelength and lie in an easily accessible spectral region, some authors have used the [N II]/Hα ratio to identify LINERs. Others have even used only the [O II] $\lambda 3727 \gtrsim$ [O III] $\lambda 5007$ criterion. One must bear in mind that these two definitions differ from the original ones established by H80 and can lead to inconsistencies; they should *not* be used when selecting a sample of genuine LINERs.

Despite the efforts of the past decade, the excitation mechanism of LINERs remains highly controversial. In classical AGNs, photoionization models which invoke a power-law, nonstellar ionizing continuum are generally successful in accounting for the gross characteristics of the broad and narrow emission lines. Because of the intrinsic weakness of LINERs and of the larger relative contamination of starlight, such a nonstellar continuum has only been detected in a few well-studied objects. Excitation mechanisms that have been proposed include photoionization by a dilute power-law continuum, shock heating, cooling flows, and photoionization by very hot Wolf-Rayet stars and normal O stars (see the review by Filippenko 1993, and references therein). The general consensus is that LINERs constitute a heterogeneous class of objects, especially when one considers objects with spatially extended ($r \gtrsim 200$ pc) emission. Quantitative evidence to substantiate this conclusion for "compact LINERs" ($r \lesssim 200$ pc), however, is not strong.

In this paper, we use high-quality optical spectra, in conjunction with other published results, to attempt to address the excitation mechanism of LINERs, specifically those with compact emission-line gas. We suggest that LINERs can best be explained by photoionization by nonstellar ionizing continua with a range of spectral hardness and gas densities. Shock heating as a viable excitation mechanism is also explored, and the possible contribution of stellar sources is discussed. The observations, data reduction, and starlight subtraction method are described in § 2. We present the observational results and theoretical calculations in § 3. A discussion of the viability of various excitation mechanisms in the context of our results can be found in § 4. Section 5 summarizes the main conclusions.

[1] Presidential Young Investigator.

[2] Note that [O II] $\lambda 3727$ designates the [O II] $\lambda\lambda 3726, 3729$ doublet, while [O III] $\lambda 5007$ and [O I] $\lambda 6300$ refer to single lines. When the occasion arises, [S II] $\lambda 6724 \equiv$ [S II] $\lambda\lambda 6716, 6731$, and [O II] $\lambda 7325 \equiv$ [O II] $\lambda\lambda 7319, 7330$.

[3] This and all subsequent line intensity ratios involving Hα only refer to the *narrow* component of the line. In some objects, an additional broad component of Hα may also be present.

TABLE 1

JOURNAL OF OBSERVATIONS

Object	Class[a]	UT Date	Exp. (s)	Aper. ($''\times''$)[b]	P.A.[c]	$\Delta\lambda_b$ (Å)[d]	$\Delta\lambda_r$ (Å)[e]	Res. (Å)[f]	sec z[g]	See[h]
NGC 221	T	1990 Feb 11	600	1 × 4	81	3380–5070	7380–9830	5.0 (8)[i]	1.4	1.5
		1990 Nov 28	200	2 × 4	77	3480–5160	5030–7480	5.0 (8)	1.6	1.5
		1990 Nov 28	60	2 × 4	77	3480–5160	5030–7480	5.0 (8)	1.6	1.5
		1990 Nov 29	100	2 × 4	77	3480–5160	7380–9830	5.0 (8)	1.7	2.0
NGC 224	T	1990 Feb 11	600	1 × 4	81	3380–5070	7380–9830	5.0 (8)	1.5	1.5
		1990 Nov 28	200	2 × 4	77	3480–5160	5030–7480	5.0 (8)	1.6	1.5
		1990 Nov 29	200	2 × 4	77	3480–5160	7380–9830	5.0 (8)	1.8	3.5
NGC 315	L	1990 Feb 10	1200	1 × 4	69	4230–5110	5030–7480	2.5 (8)	1.8	1.5
		1990 Nov 28	1200	2 × 4	71	3480–5160	5030–7480	5.0 (8)	1.4	1.5
		1990 Nov 29	1200	2 × 4	71	3480–5160	7380–9830	5.0 (8)	1.6	3.5
NGC 404	L	1990 Feb 10	1200	1 × 4	69	4230–5110	5030–7480	2.5 (8)	1.8	1.5
		1990 Feb 11	2400	1 × 4	72	3380–5070	7380–9830	5.0 (8)	1.5	1.5
NGC 1052	L	1990 Nov 28	900	2 × 4	20	3480–5160	5030–7480	5.0 (8)	1.4	2.0
		1990 Nov 28	100	2 × 4	20	3480–5160	5030–7480	5.0 (8)	1.4	2.0
		1990 Nov 29	900	2 × 4	20	3480–5160	7380–9830	5.0 (8)	1.4	2.0
NGC 1167	L	1990 Feb 10	1200	1 × 4	69	4230–5110	5030–7480	2.5 (8)	1.8	1.5
		1990 Nov 28	1500	2 × 4	82	3480–5160	5030–7480	5.0 (8)	1.2	1.5
		1990 Nov 29	1500	2 × 4	82	3480–5160	7380–9830	5.0 (8)	1.2	2.0
NGC 1275	S	1990 Feb 10	1800	1 × 4	62	4230–5110	5030–7480	2.5 (8)	1.2	1.5
		1990 Feb 10	700	1 × 4	62	4230–5110	5030–7480	2.5 (8)	1.3	1.5
		1990 Feb 11	1800	1 × 4	62	3380–5070	7380–9830	5.0 (8)	1.2	2.5
NGC 1667	S	1990 Feb 10	1800	1 × 4	45	4230–5110	5030–7480	2.5 (8)	1.7	1.5
		1990 Feb 11	2700	1 × 4	45	3380–5070	7380–9830	5.0 (8)	1.6	2.5
NGC 2639	L	1990 Feb 10	1800	1 × 4	190	4230–5110	5030–7480	2.5 (8)	1.1	1.5
		1990 Feb 11	2200	1 × 4	190	3380–5070	7380–9830	5.0 (8)	1.1	2.5
NGC 2841	L	1990 Feb 10	900	1 × 4	199	4230–5110	5030–7480	2.5 (8)	1.1	1.5
		1990 Feb 11	900	1 × 4	199	3380–5070	7380–9830	5.0 (8)	1.1	2.0
NGC 3031	L	1990 Feb 10	600	1 × 4	199	4230–5110	5030–7480	2.5 (8)	1.2	1.5
		1990 Feb 10	100	1 × 4	199	4230–5110	5030–7480	2.5 (8)	1.2	1.5
		1990 Feb 11	600	1 × 4	199	3380–5070	7380–9830	5.0 (8)	1.2	2.0
		1990 Nov 28	200	2 × 4	60	3480–5160	5030–7480	5.0 (8)	1.4	1.0
		1990 Nov 29	300	2 × 4	60	3480–5160	7380–9830	5.0 (8)	1.4	2.5
NGC 3115	T	1990 Feb 10	600	1 × 4	0	4230–5110	5030–7480	2.5 (8)	1.3	1.5
NGC 4339	T	1990 Nov 28	700	2 × 4	133	3480–5160	5030–7480	5.0 (8)	1.4	2.0
		1990 Nov 29	700	2 × 4	133	3480–5160	7380–9830	5.0 (8)	1.4	1.5
NGC 4395	S	1990 Feb 10	1200	1 × 4	85	4230–5110	5030–7480	2.5 (8)	1.1	1.5
		1990 Feb 11	1300	1 × 4	85	3380–5070	7380–9830	5.0 (8)	1.1	1.1
NGC 4618	H	1990 Nov 28	1500	2 × 4	64	3480–5160	5030–7480	5.0 (8)	1.3	2.0
		1990 Nov 29	1500	2 × 4	64	3480–5160	7380–9830	5.0 (8)	1.4	2.5
NGC 7217	L	1990 Nov 28	1200	2 × 4	76	3480–5160	5030–7480	5.0 (8)	1.2	2.0
		1990 Nov 29	800	2 × 4	76	3480–5160	7380–9830	5.0 (8)	1.3	1.5
NGC 7479	L	1990 Nov 28	1500	2 × 4	55	3480–5160	5030–7480	5.0 (8)	1.6	2.0
		1990 Nov 29	1500	2 × 4	55	3480–5160	7380–9830	5.0 (8)	1.5	1.5
NGC 7714[j]	H	1992 Jan 09	1200	2 × 5	34	3100–4670	—	6	1.4	2.0
		1992 Jan 09	600	2 × 5	39	4510–6070	—	6	1.5	2.0
		1992 Jan 09	600	2 × 5	39	5920–7510	—	6	1.6	2.0
		1992 Jan 09	600	2 × 5	39	6760–9930	—	12	1.6	2.0
NGC 7743	L	1990 Nov 28	1500	2 × 4	56	3480–5160	5030–7480	5.0 (8)	1.7	2.0
		1990 Nov 28	100	2 × 4	56	3480–5160	5030–7480	5.0 (8)	1.8	2.0
		1990 Nov 29	1200	2 × 4	56	3480–5160	7380–9830	5.0 (8)	1.7	2.0

[a] Classification of object. L = LINER, S = Seyfert, T = template galaxy, H = H II region or starburst galaxy.
[b] Effective aperture size for extraction of spectra (seconds of arc).
[c] Position angle (degrees) of slit. This was close to the parallactic angle if the object was not near the zenith.
[d] Observed spectral range for the blue camera.
[e] Observed spectral range for the red camera.
[f] Spectral resolution (full width at half-maximum intensity).
[g] Secant of zenith angle at midpoint of observation. This is approximately equal to the air mass.
[h] Visual estimate of seeing disk (FWHM, seconds of arc).
[i] First (second) value is spectral resolution for blue (red) camera.
[j] Obtained at Lick Observatory with the Shane 3 m reflector, using the Cassegrain spectrograph with a TI 800 × 800 pixel CCD. The "UV" (3100–4670 Å), "green" (4510–6070 Å), and "red" (5920–7510 Å) settings used a 600 grooves mm^{-1} grating, and the "IR" (6760–9930 Å) setting used a 300 grooves mm^{-1} grating.

2. THE NEW DATA SET

2.1. *Observations and Reductions*

Two-dimensional (long-slit) spectra were obtained on 1990 February 10–11 and November 28–29 UT with the Double Spectrograph (Oke & Gunn 1982) attached to the Cassegrain focus of the Hale 5 m telescope at Palomar Observatory. The data were obtained as a supplement to a complete, magnitude-limited, spectroscopic survey of the 500 brightest ($B_T \lesssim 12.5$ mag) galaxies north of the celestial equator (Filippenko & Sargent 1985). From the objects observed in the survey, we selected a subset of galaxies to be studied in detail. This subset consists of 13 LINERs, three Seyfert nuclei, one emission-line galaxy with nuclear H II regions, and four absorption-line galaxies. We also included in our sample a spectrum of the starburst galaxy NGC 7714, obtained with the Shane 3 m telescope at Lick Observatory on 1992 January 9 UT. A journal of observation is given in Table 1.

A long slit of width 1″ (2″ for the November run) was placed across the nucleus of each galaxy. The slit was generally oriented along the parallactic angle in order to minimize light losses due to atmospheric dispersion (Filippenko 1982); if the galaxy was near the zenith (sec $z \lesssim 1.1$), the slit was sometimes rotated to a more astrophysically interesting angle. A dichroic filter located behind the slit reflected light with $\lambda \lesssim 5500$ Å to the "blue camera" and transmitted light with $\lambda \gtrsim 5500$ Å to the "red camera." Two-dimensional spectra were recorded on TI CCDs of 800 × 800 square pixels. The spatial resolution of the red camera was 0.58 arcsec pixel^{-1}, while that of the blue camera was 0.40 and 0.80 arcsec pixel^{-1} for the February and November runs, respectively.

For the first night of the February run, the approximate wavelength ranges 4230–5110 Å (blue camera, 600 grooves mm^{-1} grating) and 5030–7480 Å (red camera, 316 grooves mm^{-1} grating) were observed simultaneously, with a resolution (FWHM) of 2.5 and 8 Å, respectively. For the second night, the blue camera covered 3380–5070 Å (300 grooves mm^{-1} grating) with 5 Å resolution, while the red camera covered 7380–9830 Å (316 grooves mm^{-1} grating) with 8 Å resolution. The setup for both nights of the November run was very similar, with the blue camera covering 3480—5160 Å. Typical integration times were 900–1800 s in order to achieve signal-to-noise (S/N) ratios of at least 100/1 in the nucleus.

The bias level of each data frame, recorded as a single number for every column along the dispersion, was subtracted. Pixel-to-pixel variations in the response of the CCD were removed with appropriately normalized dome flat fields. During the reduction procedure, slight tilts of the spectra with

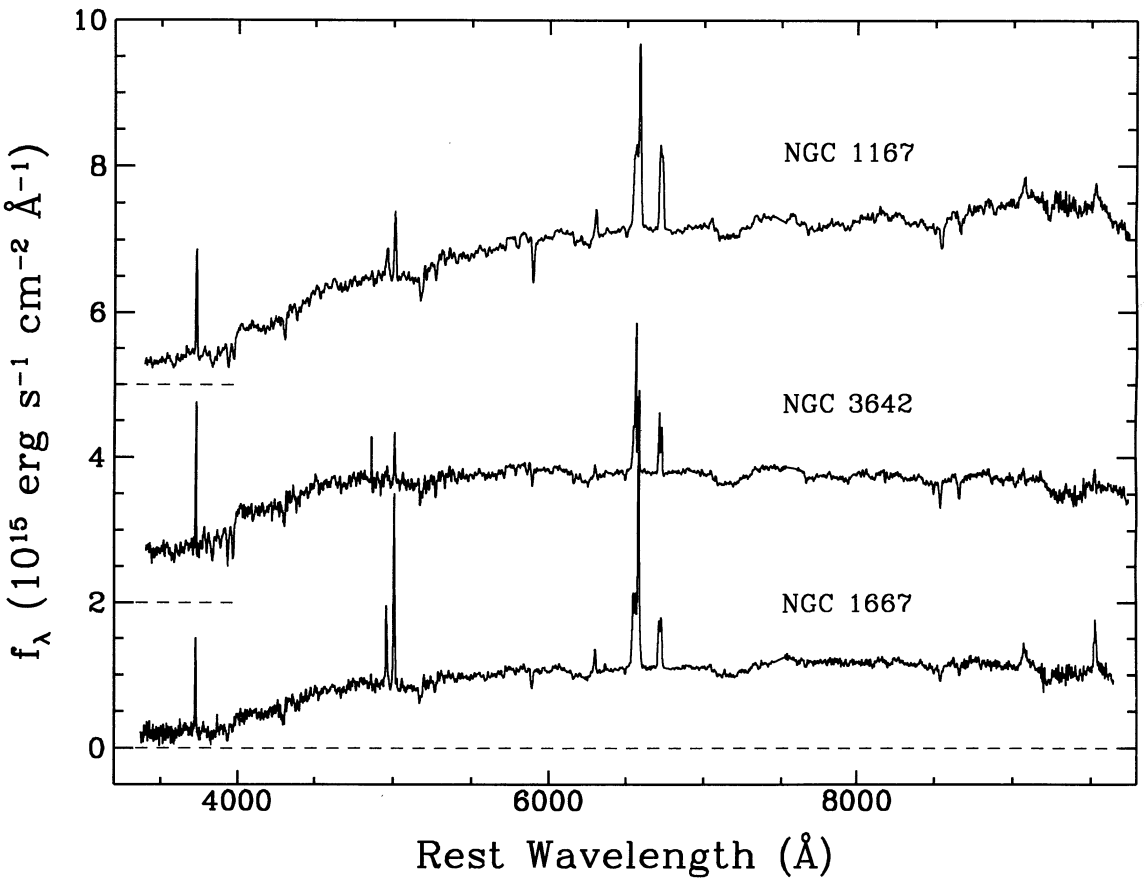

FIG. 1*a*

FIG. 1.—Flux-calibrated spectra of the observed galaxies. The ordinate represents the flux density (f_λ in units of 10^{15} ergs s^{-1} cm^{-2} Å^{-1}); an additive constant has been added to each galaxy for display purposes. The dashed, horizontal lines denote the zero level of each galaxy. The wavelengths have been shifted to the rest frame of the galaxies. Imperfectly removed residuals at the band heads of the atmospheric A band ($\lambda \approx 7580$ Å) and B band ($\lambda \approx 6860$ Å) have been eliminated by interpolation (shown as a straight line). (*a*) NGC 1167, 3642, and 1667. (*b*) NGC 404, 2639, 3642, and 7743. (*c*) NGC 3998, 2841, 1052, and 1275. (*d*) NGC 3031 (M81), 7714, and 3504; the spectrum of NGC 7714 has been scaled by a factor of 0.15 for display purposes. (*e*) NGC 315, 7479, and 4618.

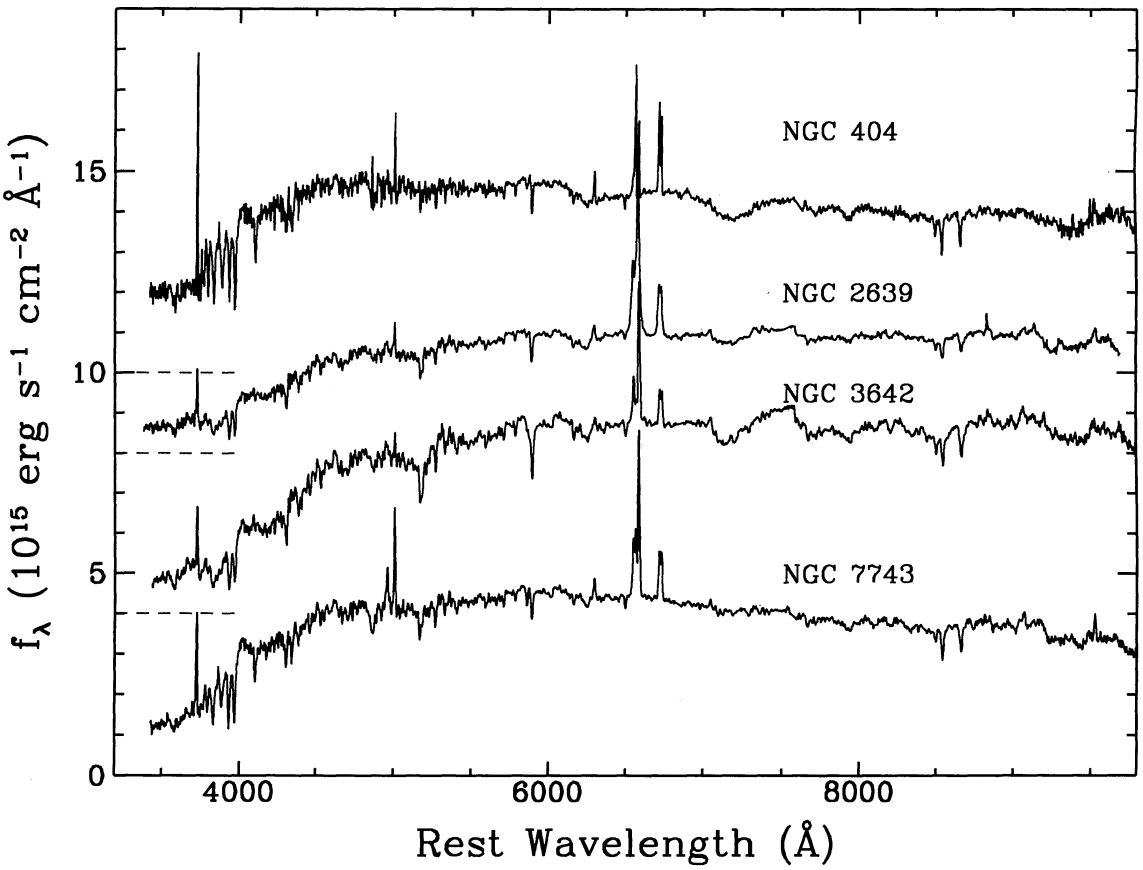

FIG. 1*b*

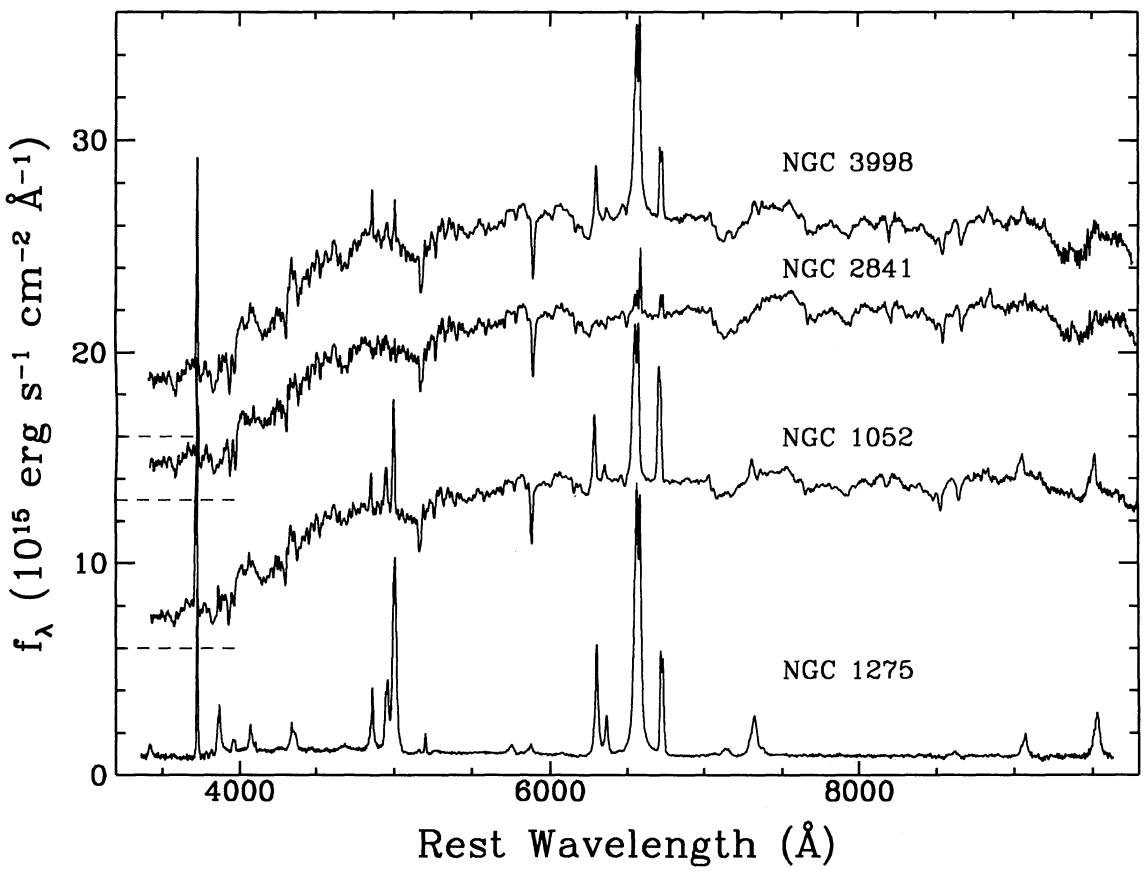

FIG. 1*c*

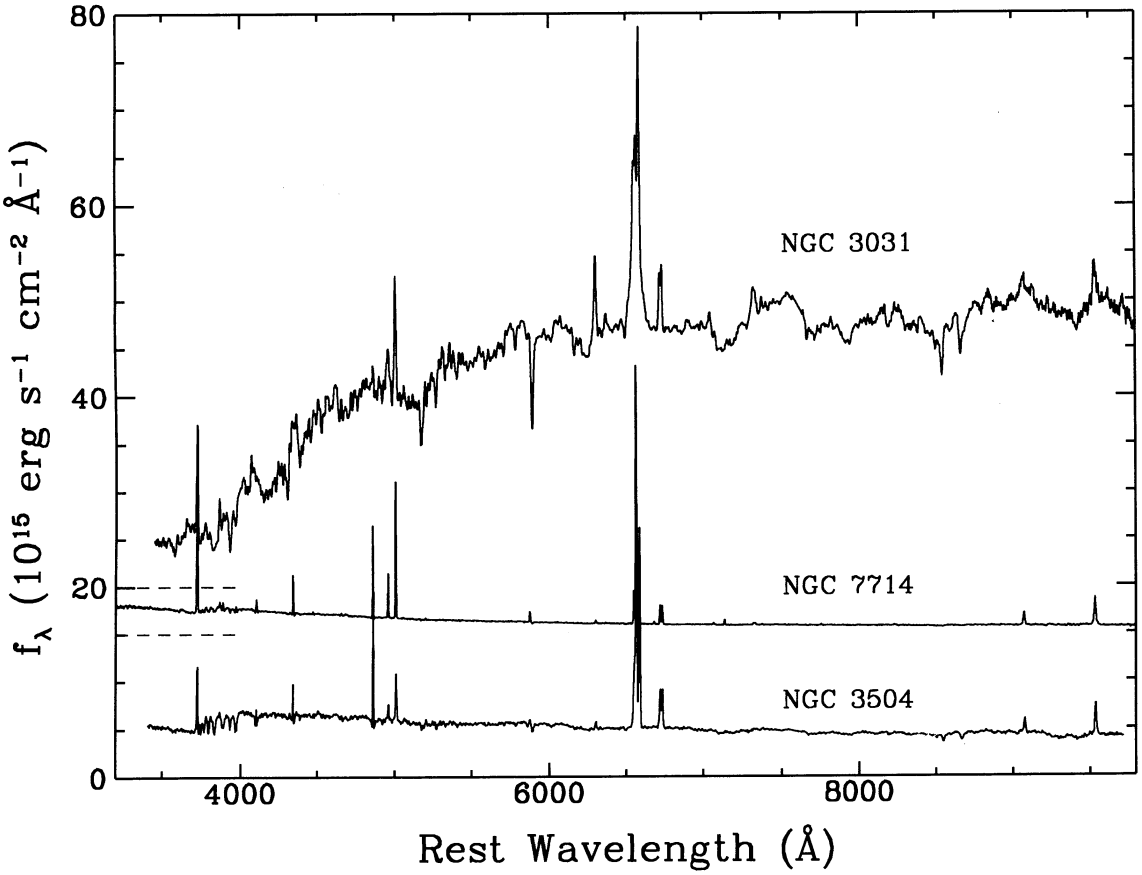

FIG. 1*d*

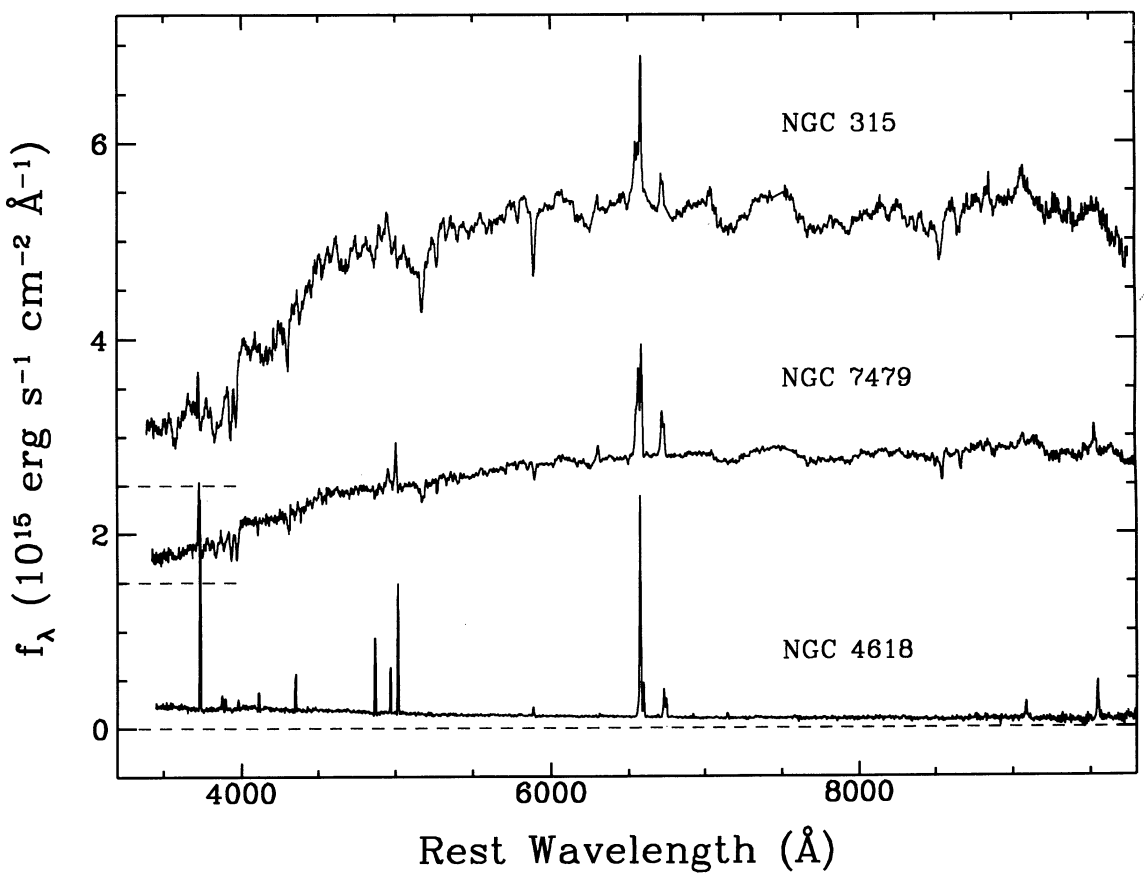

FIG. 1*e*

respect to a straight column of pixels were removed by fitting a cubic spline. We extracted one-dimensional spectra of the nucleus of each object by summing over the central 10 pixels of the blue CCD (except for the November run, in which the central 5 pixels were summed), and the central 7 pixels of the red CCD. Thus, the effective aperture achieved for the February run was $\sim 1'' \times 4''$, and that of the November run was $\sim 2'' \times 4''$.

The background sky level was determined from two regions, one close to and the other far from the nucleus of each object. In almost all cases, the levels of the two were nearly identical. Any spurious pixel values introduced by cosmic rays were automatically removed in the process.

Spectra of bright secondary standard stars (Oke & Gunn 1983; Massey et al. 1988) were used to calibrate the relative and absolute fluxes of the spectra. Telluric oxygen absorption lines near 6280 Å, 6860 Å (the "B band"), and 7580 Å (the "A band"), as well as the water absorption lines near 9400 Å and elsewhere, were removed by division of normalized, intrinsically featureless spectra of the standards. Large residuals caused by mismatches at the strong band heads were eliminated by interpolation in the plotted spectra. For those spectra that extended beyond 3420 Å in the blue, we removed the ozone bands (Schachter 1991) with the division of a spectrum of a sdO star. The reduction procedure also corrected for continuum atmospheric extinction.

We established the wavelength scale by fitting a cubic or quartic polynomial to unblended emission lines of He, Ne, Ar, Hg, and Fe in the comparison lamp spectra taken throughout the observations. These spectra were also used to measure the spectral resolution as a function of position on the CCDs, which is necessary in order to remove the instrumental resolution from the measured line widths.

For each galaxy, multiple exposures taken with the same setting were combined in a weighted average, with the weights determined by the exposure time and seeing conditions. The spectra from the different wavelength settings were then concatenated after averaging the overlapping regions and scaling the blue and near-infrared spectra to the red spectrum, which generally had the higher S/N ratio. The combined flux- and wavelength-calibrated spectra are plotted in Figure 1; each galaxy has been shifted to its rest frame.

2.2. *Starlight Subtraction*

The spectra of our emission-line galaxies are heavily contaminated, and in some cases dominated, by the underlying starlight. In order to get accurate measurements of line fluxes, it is imperative that the starlight be properly removed. The detection of some weak narrow lines, as well as identification of weak, broad Hα emission, hinges on this procedure.

Previous workers have used various techniques to remove the starlight. Fosbury et al. (1978) subtracted an off-nuclear spectrum (mostly devoid of emission features) from the spectrum of the nucleus of NGC 1052. Keel (1983a), on the other hand, generated synthetic spectra of the underlying starlight by spectral synthesis techniques. Finally, a frequently used procedure is to subtract from the object spectrum a spectrum of an absorption-line "template" galaxy (e.g., Stauffer 1982; Phillips, Charles, & Baldwin 1983; Filippenko & Halpern 1984; Filippenko & Sargent 1988). In this work, we adopt the last approach.

Our technique closely follows that of Filippenko & Halpern (1984) and Filippenko & Sargent (1988). The template galaxies we use are NGC 221 (M32), NGC 224 (M31), NGC 4339, and NGC 3115. They vary in properties such as internal reddening (which affects the overall continuum shape), velocity dispersion, metallicity, and, to a lesser degree, stellar population. This variation provides a useful range of properties with which to match our object spectra (Fig. 2). In our final results, the template galaxy that best matches the underlying starlight of the object spectrum, and thus yields the smallest residuals, is chosen empirically by trial and error. NGC 4339 and NGC 3115 provide the closest match for most of the galaxies in our sample; NGC 221 is used in some objects where the metallicity is higher.

The method to subtract the template spectrum from the object spectrum consists of the following steps:

1. Correct the spectra for Galactic reddening using the extinction values of Burstein & Heiles (1984) and the extinction curve of Cardelli, Clayton, & Mathis (1989).
2. Remove the redshifts by determining the observed wavelengths of several unblended absorption lines.
3. Determine a wavelength-dependent scaling factor for the template spectrum by fitting a cubic spline through several representative points in the ratio of the object spectrum to the template spectrum, taking care not to include regions with known emission lines.
4. Multiply the template spectrum by the wavelength-dependent scaling factor.
5. Separate the object and template spectra into roughly 10 small intervals of ~ 400 Å width.
6. Examine in detail how well the template matches the continuum and absorption lines of the object in each of the wavelength intervals. If the metallicity of the template does not match that of the object, the absorption features are either diluted or strengthened by adding or subtracting (respectively) a suitably scaled, constant local continuum.
7. Apply small, local shifts in wavelength (caused by small errors in wavelength calibration or redshift) to the template spectrum in order to minimize mismatches with the object spectrum.
8. Subtract the template spectrum from the object spectrum.
9. Concatenate the various wavelength intervals into a final spectrum covering the original spectral range. Figure 3 illustrates the effectiveness of this method for NGC 3998 and NGC 1667, for which NGC 3115 and NGC 4339 (respectively) were chosen as template galaxies.

We have found that the method outlined above works reasonably well for objects whose stellar population matches that of the templates, mainly F–K stars. Certain objects in our sample, however, have substantially younger stars in their nucleus, as evidenced by the presence of strong Balmer absorption lines in their spectra. These galaxies are NGC 404, NGC 3504, and, to a lesser extent, NGC 7743. NGC 3504 also exhibits a substantial blue continuum. For such objects, the template subtraction method works poorly for $\lambda \lesssim 5800$ Å, since the young stars contribute mostly in the blue, but it is much less affected for $\lambda \gtrsim 5800$ Å. In order to obtain a rough measurement of the strongest lines at $\lambda \lesssim 5800$ Å in these objects, we simply fit a spline by eye to the continuum level. More accurate measurements will have to await more refined techniques, perhaps spectral synthesis using a stellar library (e.g., Silva 1991) or a library of observed star cluster spectra (e.g., Bica 1988).

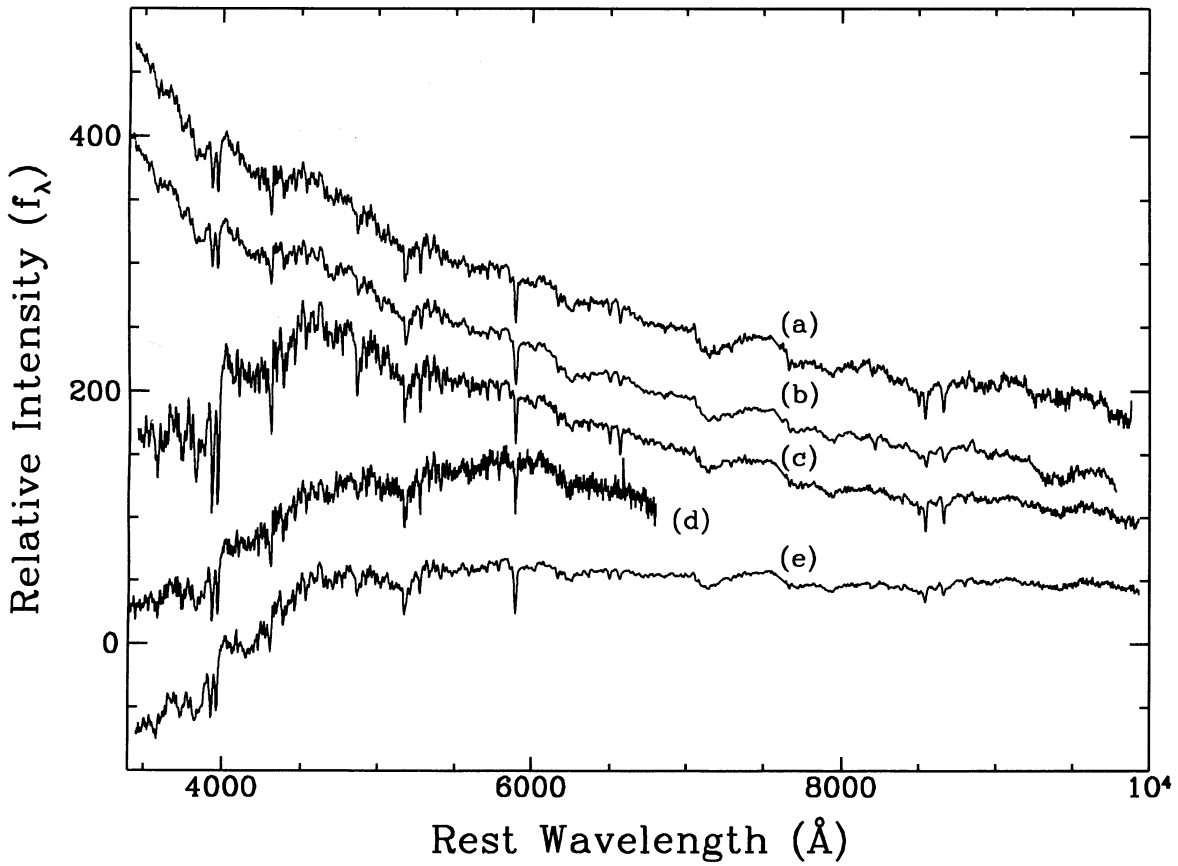

FIG. 2.—Template galaxies used for starlight removal of program galaxies. The redshift of each object has been removed, as has the Galactic extinction. The spectra have been scaled such that the Na D line has roughly the same strength. Spectrum (a) corresponds to NGC 4339 (× 50), (b) NGC 3115 (× 4), (c) NGC 221 (× 1), (d) IC 4889 (× 20), and (e) NGC 224 (× 1.33). Residuals in the A and B bands have been removed by interpolation.

2.3. *Line Measurements*

The intensities and line widths were measured interactively by marking the endpoints and FWHM of a line with a cursor. This method was chosen over that of fitting an analytic function to the line profile because the line profiles are often asymmetrical or do not have pure Gaussian or Lorentzian shapes. For lines that are slightly blended in a few cases, we attempted to fit Gaussians, if this appeared to yield more reasonable values. This applied to the following lines: [S II] λ4073 and Hδ, [O I] λ6300 and [O I] λ6364, and [O I] λ6300 and [S III] λ6312.

The Hα + [N II] and [S II] lines pose a special problem in the red spectral region, since these are partially blended by the spectral resolution of our observations or by internal broadening. Moreover, many objects in our sample show evidence for a broad component of Hα emission, which complicates the decomposition of the blend. The measurement of the Hα flux is especially critical, as it is used to determine the Balmer decrement used for reddening corrections (§ 2.4) and it plays a prominent role in our analysis of the results. Accordingly, we used the higher dispersion data of Filippenko & Sargent (1985) to deconvolve these lines. We removed the starlight contamination from the Filippenko & Sargent (1985) spectra in the same manner described above, using NGC 4339 as the template galaxy for all the objects. In objects which show an obvious presence of broad Hα emission, we approximated the broad component with a cubic spline and subtracted it from the Hα + [N II] blend. The relative line fluxes were then determined either interactively or by fitting Gaussians; the latter was necessary in cases where the intrinsically wide lines are still not completely unblended. Finally, we applied the relative contribution of each line to the respective blends to determine the fluxes in our original (lower dispersion) spectra.

2.4. *Reddening Correction*

All the line fluxes given in this paper have been corrected for internal and Galactic reddening (Burstein & Heiles 1984), using the reddening curve of Cardelli et al. (1989). The amount of internal reddening was determined by comparing the observed Balmer decrement to the theoretical value for case B recombination. In the case of NGC 4618 and NGC 7714, whose spectra are dominated by H II regions, this value was taken to be $H\alpha/H\beta = 2.85$ for $n_e = 10^4$ cm^{-3} and $T_e = 10^4$ K (Brocklehurst 1971). For the LINERs and Seyferts in our sample, we assumed $H\alpha/H\beta = 3.1$, a value more suitable for AGN environments in which collisional excitation tends to enhance Hα (Halpern & Steiner 1983; Ferland & Netzer 1983; Péquignot 1984).

We note, however, that the reddening correction is uncertain, because it depends on the accuracy of our line measurements, which, in turn, depends on the accuracy of the starlight subtraction procedure. In particular, several of the objects in our sample have fairly steep measured Balmer decrements. We cannot, of course, a priori rule out that these objects are sub-

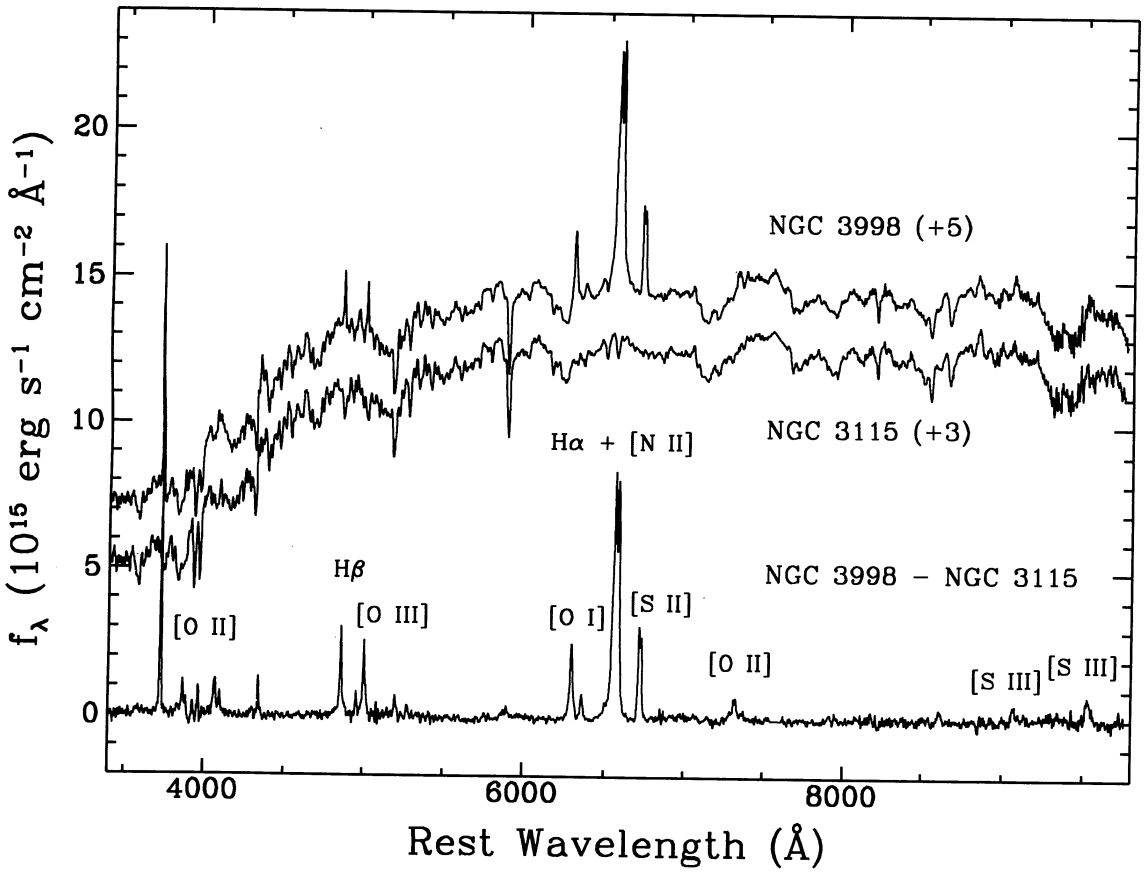

FIG. 3*a*

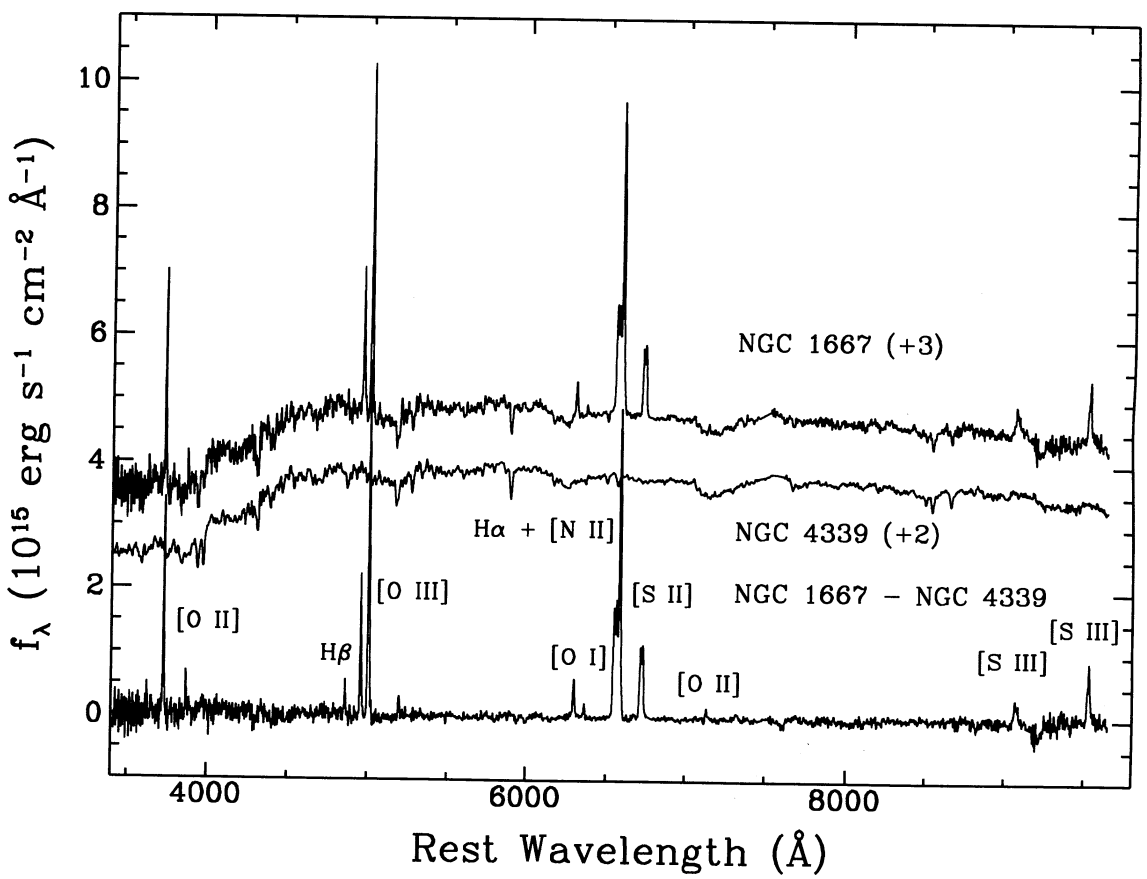

FIG. 3*b*

stantially reddened, either because of increased amounts of dust in their narrow-line region (NLR) or because they are highly inclined. It is well known, for example, that narrow-line X-ray galaxies tend to be very reddened, and that the amount of reddening is correlated with the inclination and inversely correlated with the measured luminosity of the galaxy (Lawrence & Elvis 1982). H80 and others note that LINERs tend to have relatively large Balmer decrements. It must be borne in mind, however, that these previous results may be uncertain due to incomplete treatment of the starlight contamination.

The fluxes of emission lines relative to Hβ, both as observed and corrected for reddening, are given in Table 2. These measurements will be used for the comparison with the photoionization and shock calculations in § 3. The last row gives the assumed reddening correction factor. The uncertainty of the line fluxes listed, especially for the weaker lines, depends critically on the accuracy of the starlight subtraction and is thus difficult to assess quantitatively. Based on repeated applications of the method outlined in § 2.2, we estimate that measurements of the relative strengths of strong lines (such as those used in our analysis below) are accurate to $\sim$10% for bright objects (e.g., NGC 3031) and $\sim$30% for faint ones (e.g., NGC 315). Weaker lines such as [Ne III] λ3869, [N I] λ5200, or [Ar III] λ7136 are likely to be uncertain by $\sim$30%–50% for bright and faint objects, respectively.

In order to enlarge the data sample, our subsequent analysis will also make use of additional data obtained from the literature (Table 3); all objects combined will be referred to as the "combined sample." Only objects which could be reliably classified by H80's criteria were chosen; consequently, we did not include Mrk 739, Mrk 1158, and Ark 160 from the sample of Ferland & Netzer (1983). Close inspection of a few objects that are common to our new sample indicates that the quality of our spectra is generally better and that our starlight removal is more accurate. Thus, we place greater confidence in our measurements of the line fluxes and reddening corrections. For the purposes of the present study, we simply adopt the line measurements and reddening corrections quoted by the respective authors. However, we emphasize that it is preferable to have a large database observed with fairly uniform S/N ratio and corrected for starlight contamination in a systematic manner. We are currently attempting to obtain such a sample of observations.

3. RESULTS

3.1. *New Photoionization Calculations*

Previous photoionization studies have emphasized that the general properties of the emission-line spectra of LINERs can be reproduced by a power-law ionizing continuum similar to that thought to occur in Seyfert 2 nuclei, but with an ionization parameter U (the ratio of the ionizing photon density to nucleon density at the face of the cloud) which is smaller ($\sim 10^{-3.5}$ instead of $10^{-2.5}$; Ferland & Netzer 1983; Halpern & Steiner 1983). In the standard AGN paradigm, this power-law ionizing continuum arises from the vicinity of a supermassive compact object, presumably a black hole (Rees 1984, and references therein). An alternative explanation invokes hot, massive Wolf-Rayet stars ("Warmers") in a metal-rich starburst environment to provide the high-energy photons (Terlevich & Melnick 1985). This scenario was largely motivated by the similarity between the ionizing continuum of a cluster of Warmers and a power law with a spectral index $\alpha = -1.5$ (where $f_\nu \propto \nu^\alpha$), which is usually invoked for Seyfert 2 nuclei and LINERs (Ferland & Netzer 1983; Halpern & Steiner 1983). However, Leitherer, Gruenwald, & Schmutz (1992) find that more realistic models of Wolf-Rayet stars that take into account non-LTE atmospheres are unable to produce enough high-energy photons to account for AGN spectra; their results seriously challenge the conclusions of Terlevich & Melnick (1985).

Another alternative based on photoionization models using O-type stars proposes that some LINERs (Filippenko & Terlevich 1992; see also Ho & Filippenko 1993), or perhaps many LINERs (Shields 1992), may in fact be simply nuclear H II regions. If true, these findings have important consequences. They imply that a significant fraction of LINERs should not be considered genuine AGNs. Normal star formation, rather than accretion onto a massive black hole, would be all that is needed to explain these objects.

To explore these ideas in greater detail in light of our new data, we generated theoretical photoionization calculations using the code CLOUDY (Ferland 1991) for a nonstellar ionizing continuum which we represent as a power law with a range of spectral indices. The code solves the equations of statistical and thermal equilibrium and calculates a self-consistent model for the values of the temperature and ionization as a function of depth into a gas cloud. The geometry of the cloud that represents the gas in the NLR was assumed to be plane parallel. Although we assumed that the gas has a constant density, we generated a sequence of models in which the total hydrogen density n was set to $10^{2.5}$, 10^3, 10^4, 10^5, and 10^6 cm^{-3} in order to investigate the effect of variations in density. We have verified that keeping the total pressure (rather than the density) constant changes the optical line intensity ratios by at most 10%–15% for values of U appropriate for LINERs. In our calculations, we adopted solar abundances (Grevesse & Anders 1989) for the set of 13 elements included (H, He, C, N, O, Ne, Mg, Al, Si, S, Ar, Ca, Fe). We neglected the effect of dust grains on the depletions of the elements and their contributions to the cooling and heating functions. Inclusion of depletion onto dust grains modifies the relative contribution of different elements to the cooling function and consequently changes various line intensity ratios of the emission-line spectrum (Shields 1992). We have verified that the main conclusions of this study do not depend on the effect of depletions. Dust grains do have significant effects on the cooling and heating of the gas, but only for $\log U > -2$ (Ferland 1993).

For each value of n, models were generated for a grid of values for U and α: $\log U = -2.5$, -3, -3.5, -4, -4.5, and -5; $\alpha = -1$, -1.5, -2, and -2.5. The slope of the power law at low energies ($\lambda \gtrsim 10$ μm) was assumed to be $\alpha = 2.5$, appropriate for a self-absorbed synchrotron continuum. The high-energy slope ($\gtrsim$50 keV) is constrained by the contribution of

FIG. 3.—(*a*) Illustration of starlight removal procedure for NGC 3998 using the template galaxy NGC 3115. The ordinate is in units of 10^{15} ergs s^{-1} cm^{-2} Å^{-1}. *Top*: NGC 3998 before subtraction (offset by +5 units). *Middle*: NGC 3115 offset by +3 units. *Bottom*: Final spectrum of NGC 3998 after subtracting the template from the original spectrum. The prominent emission lines are labeled for reference. (*b*) The same procedure for NGC 1667 using the template galaxy NGC 4339. *Top*: NGC 1667 before subtraction (offset by +3 units). *Middle*: NGC 4339 offset by +2 units. *Bottom*: Final spectrum of NGC 1667 after subtracting the template from the original spectrum.

TABLE 2

EMISSION-LINE INTENSITIES OF OBSERVED GALAXIES[a]

Line	NGC 315		NGC 404		NGC 1052		NGC 1167		NGC 1275	
(Å)	$F(\lambda)/F(H\beta)$		$F(\lambda)/F(H\beta)$		$F(\lambda)/F(H\beta)$		$F(\lambda)/F(H\beta)$		$F(\lambda)/F(H\beta)$	
[Ne V] λ3426	—	—	—	—	—	—	0.05	0.05	0.66	0.91
[O II] λ3727	5.37	10.02	6.04	6.85	3.28	3.28	6.58	6.58	2.77	3.58
[Ne III] λ3869	1.58	2.74	—	—	0.29	0.29	0.64	0.64	1.51	1.89
[Ne III] λ3970[b]	—	—	—	—	0.25	0.25	0.36	0.36	0.33	0.41
[S II] λ4073	—	—	—	—	0.32	0.32	0.29	0.29	0.68	0.82
Hδ λ4102	0.46	0.74	—	—	0.11	0.11	0.24	0.24	0.09	0.11
Hγ λ4340	0.49	0.66	—	—	0.33	0.33	0.25	0.25	0.56	0.64
[O III] λ4363	—	—	—	—	0.12	0.12	0.025	0.025	0.35	0.38
He II λ4686	—	—	—	—	—	—	—	—	0.27	0.28
Hβ λ4861	1.00	1.00	1.00	1.00	1.00	1.00	1.00	1.00	1.00	1.00
[O III] λ4959	1.07	1.01	0.69	0.69	0.72	0.72	1.01	1.01	1.39	1.34
[O III] λ5007	1.27	1.17	1.39	1.39	1.98	1.98	2.77	2.77	3.79	3.63
[N I] λ5200	—	—	0.26	0.26	0.04	0.04	0.22	0.22	0.14	0.13
Fe II λ5270	1.06	1.01	0.63	0.63	0.10	0.10	0.28	0.28	0.08	0.08
[Fe VII] λ5721	—	—	—	—	0.02	0.02	—	—	0.023	0.019
[N II] λ5755	—	—	—	—	0.04	0.04	0.13	0.13	0.12	0.10
He I λ5876	—	—	0.21	0.19	0.002	0.002	0.12	0.12	0.14	0.11
[O I] λ6300	2.04	1.19	0.76	0.71	1.35	1.35	0.94	0.94	1.95	1.54
[O I] λ6364	0.45	0.26	0.33	0.31	0.32	0.32	0.26	0.26	0.61	0.49
[N II] λ6548	2.49	1.37	0.49	0.43	0.97	0.97	1.94	1.94	0.42	0.31
Hα λ6563	5.64	3.08	3.51	3.04	2.82	2.82	2.49	2.49	2.91[c]	2.18[c]
[N II] λ6583	10.71	5.86	1.76	1.52	2.86	2.86	5.13	5.13	1.23	0.93
He I λ6678	—	—	—	—	0.03	0.03	0.07	0.07	—	—
[S II] λ6716	6.11[d]	3.18[d]	2.01	1.74	3.04[d]	3.04[d]	2.04	2.04	0.88[d]	0.66[d]
[S II] λ6731	—	—	1.61	1.39	—	—	2.04	2.04	—	—
[Ar III] λ7136	—	—	0.19	0.16	0.16	0.16	0.23	0.23	0.11	0.08
[O II] λ7325	—	—	0.20	0.18	0.51	0.51	0.18	0.18	0.56	0.39
[S III] λ9069	0.09	0.03	0.031	0.027	0.61	0.61	0.45	0.45	0.16	0.09
[S III] λ9532	0.43	0.12	0.51	0.41	0.73	0.73	0.59	0.59	0.33	0.19
$F(H\beta)$[e]	0.29	2.17	1.79	2.69	5.93	5.93	2.51	2.51	74.73	179.4
c†	0.79	—	0.16	—	0	—	0	—	0.34[f]	—

Line	NGC 1667		NGC 2639		NGC 2841		NGC 3031		NGC 3504	
(Å)	$F(\lambda)/F(H\beta)$		$F(\lambda)/F(H\beta)$		$F(\lambda)/F(H\beta)$		$F(\lambda)/F(H\beta)$		$F(\lambda)/F(H\beta)$	
[Ne V] λ3426	0.39	0.97	—	—	—	—	—	—	—	—
[O II] λ3727	5.78	12.08	4.56	13.68	3.08	3.55	3.64	3.94	0.82	1.18
[Ne III] λ3869	0.99	1.98	0.33	0.89	0.25	0.29	1.49	1.62	—	—
[Ne III] λ3970[b]	0.65	1.17	0.09	0.24	—	—	1.26	1.37	—	—
[S II] λ4073	—	—	0.33	0.74	0.20	0.22	1.75	1.89	—	—
Hδ λ4102	0.48	0.83	0.05	0.11	0.13	0.14	0.68	0.74	0.11	0.14
Hγ λ4340	0.48	0.83	0.15	0.25	0.46	0.49	2.61[g]	2.84[g]	0.29	0.35
[O III] λ4363	—	—	—	—	—	—	0.88[g]	0.95[g]	0.042	0.049
He II λ4686	—	—	—	—	—	—	—	—	—	—
Hβ λ4861	1.00	1.00	1.00	1.00	1.00	1.00	1.00	1.00	1.00	1.00
[O III] λ4959	4.39	3.99	0.59	0.54	0.42	0.42	1.47	1.47	0.19	0.19
[O III] λ5007	12.34	11.10	3.79	3.32	1.51	1.51	4.67	4.67	0.68	0.63
[N I] λ5200	0.61	0.49	0.57	0.43	0.46	0.46	0.14	0.14	—	—
Fe II λ5270	—	—	0.19	0.14	0.08	0.08	0.18	0.18	—	—
[Fe VII] λ5721	0.13	0.08	—	—	—	—	—	—	—	—
[N II] λ5755	0.18	0.11	0.12	0.06	—	—	0.44	0.44	—	—
He I λ5876	—	—	—	—	—	—	—	—	—	—
[O I] λ6300	1.78	0.94	1.89	0.77	0.69	0.64	3.55	3.55	0.15	0.11
[O I] λ6364	0.49	0.26	0.61	0.23	—	—	0.89	0.89	0.07	0.05
[N II] λ6548	4.39	2.11	8.61	2.96	1.65	1.52	2.39	2.39	0.95	0.65
Hα λ6563	6.29	3.03	8.67	2.98	3.39	3.13	3.19	3.19	4.37	3.00
[N II] λ6583	13.67	6.59	20.05	6.89	5.37	4.95	7.10	7.10	2.79	1.92
He I λ6678	—	—	—	—	—	—	0.19	0.19	—	—
[S II] λ6716	6.23[d]	2.86[d]	5.46	1.88	1.90	1.75	1.77	1.77	0.71	0.49
[S II] λ6731	—	—	5.03	1.57	1.56	1.44	2.14	2.14	0.52	0.36
[Ar III] λ7136	0.36	0.14	0.70	0.19	0.17	0.16	0.44	0.40	0.10	0.07
[O II] λ7325	0.33	0.12	0.46	0.11	0.17	0.15	1.95	1.78	0.04	0.20
[S III] λ9069	1.25	0.29	0.86	0.11	0.27	0.23	0.61	0.56	0.26	0.13
[S III] λ9532	3.47	0.76	2.30	0.27	0.22	0.19	2.54	2.33	0.12	0.05
$F(H\beta)$[e]	0.49	5.35	0.48	15.39	0.63	0.81	6.38	7.65	7.62	24.39
c†	0.93	—	1.35	—	0.12	—	0.09[h]	—	0.45	—

TABLE 2.—*Continued*

Line	NGC 3642		NGC 3998		NGC 4395		NGC 4618		NGC 7217	
(Å)	$F(\lambda)/F(H\beta)$		$F(\lambda)/F(H\beta)$		$F(\lambda)/F(H\beta)$		$F(\lambda)/F(H\beta)$		$F(\lambda)/F(H\beta)$	
[Ne V] λ3426	—	—	—	—	0.85	0.85	—	—	—	—
[O II] λ3727	2.49	2.87	3.91	5.97	1.81	1.81	2.75	3.43	5.46	5.46
[Ne III] λ3869	0.89	0.97	0.79	1.17	0.65	0.65	0.15	0.18	0.22	0.22
[Ne III] λ3970[b]	0.55	0.59	0.42	0.59	0.29	0.29	0.11	0.13	0.49	0.49
[S II] λ4073	0.19	0.20	1.09	1.49	0.19	0.19	0.06	0.07	0.24	0.24
Hδ λ4102	0.22	0.24	0.52	0.70	0.16	0.16	0.25	0.29	0.32	0.32
Hγ λ4340	0.68	0.73	0.57	0.71	0.37	0.37	0.44	0.48	0.85	0.85
[O III] λ4363	—	—	—	—	0.21	0.21	—	—	—	—
He II λ4686	—	—	—	—	0.18	0.18	0.04	0.04	—	—
Hβ λ4861	1.00	1.00	1.00	1.00	1.00	1.00	1.00	1.00	1.00	1.00
[O III] λ4959	0.35	0.35	0.43	0.42	2.18	2.18	0.60	0.57	0.58	0.58
[O III] λ5007	1.72	1.72	2.12	2.01	6.73	6.73	1.73	1.64	1.79	1.79
[N I] λ5200	0.25	0.25	0.44	0.39	0.04	0.04	—	—	0.24	0.24
Fe II λ5270	0.19	0.19	0.24	0.21	0.03	0.03	—	—	—	—
[Fe VII] λ5721	—	—	—	—	—	—	—	—	—	—
[N II] λ5755	0.15	0.15	0.06	0.05	—	—	—	—	—	—
He I λ5876	0.18	0.18	0.12	0.09	0.15	0.15	0.13	0.11	—	—
[O I] λ6300	0.38	0.35	2.44	1.74	0.78	0.78	0.04	0.03	0.54	0.54
[O I] λ6364	0.13	0.12	0.64	0.44	0.28	0.28	—	—	0.22	0.22
[N II] λ6548	0.52	0.48	1.21	0.79	0.19	0.19	0.19	0.16	1.99	1.99
Hα λ6563	3.37	3.11	4.61	3.03	2.24	2.24	3.61	2.89	1.99	1.99
[N II] λ6583	1.54	1.42	3.73	2.46	0.59	0.59	0.59	0.47	6.12	6.12
He I λ6678	—	—	—	—	0.03	0.03	0.04	0.03	—	—
[S II] λ6716	1.64	1.52	1.61	1.06	0.79	0.79	0.49	0.39	1.57	1.57
[S II] λ6731	1.27	1.17	1.73	1.14	0.79	0.79	0.28	0.22	1.39	1.39
[Ar III] λ7136	0.30	0.28	0.06	0.04	0.16	0.11	0.09	0.06	—	—
[O II] λ7325	0.26	0.24	0.78	0.45	0.23	0.23	0.06	0.05	—	—
[S III] λ9069	0.47	0.39	0.49	0.22	0.45	0.45	0.41	0.27	0.09:	0.09:
[S III] λ9532	0.66	0.56	0.99	0.42	1.19	1.19	0.94	0.61	—	—
$F(H\beta)$[e]	0.51	0.66	2.39	9.06	1.87	1.87	0.59	1.17	2.02	2.02
c[†]	0.11	—	0.52	—	0	—	0.27	—	0	—

Line	NGC 7479		NGC 7714		NGC 7743	
(Å)	$F(\lambda)/F(H\beta)$		$F(\lambda)/F(H\beta)$		$F(\lambda)/F(H\beta)$	
[Ne V] λ3426	—	—	0.02	0.03	—	—
[O II] λ3727	4.99	10.08	2.06	2.33	8.65	20.17
[Ne III] λ3869	1.59	3.05	0.16	0.18	6.29	13.86
[Ne III] λ3970[b]	—	—	0.055	0.062	1.36	2.71
[S II] λ4073	—	—	0.05	0.06	1.46	2.72
Hδ λ4102	—	—	0.17	0.19	—	—
Hγ λ4340	—	—	0.42	0.45	—	—
[O III] λ4363	—	—	0.019	0.02	—	—
He II λ4686	—	—	0.06	0.06	0.21	0.24
Hβ λ4684	1.00	1.00	1.00	1.00	1.00	1.00
[O III] λ4959	0.90	0.85	0.52	0.52	3.46	3.23
[O III] λ5007	3.29	3.05	1.57	1.57	8.05	6.98
[N I] λ5200	0.52	0.43	0.03	0.03	1.76	1.40
Fe II λ5270	0.55	0.44	—	—	0.77	0.56
[Fe VII] λ5721	0.14	0.09	—	—	—	—
[N II] λ5755	0.16	0.11	—	—	0.29	0.17
He I λ5876	—	—	0.13	0.12	—	—
[O I] λ6300	1.04	0.58	0.05	0.05	2.01	0.98
[O I] λ6364	0.29	0.16	0.02	0.02	0.51	0.24
[N II] λ6548	2.28	1.19	0.41	0.36	4.05	1.81
Hα λ6563	6.05	3.09	3.34	2.89	6.92	3.09
[N II] λ6583	8.55	4.37	1.22	1.06	12.44	5.47
He I λ6678	—	—	0.034	0.029	0.21	0.09
[S II] λ6716	3.68	1.79	0.28	0.24	3.84	1.61
[S II] λ6731	2.17	1.06	0.27	0.24	3.50	1.47
[Ar III] λ7136	0.30	0.13	0.08	0.07	1.25	0.45
[O II] λ7325	0.22	0.09	0.064	0.056	0.58	0.19
[S III] λ9069	0.69	0.18	0.34	0.29	1.14	0.23
[S III] λ9532	1.52	0.37	0.83	0.67	2.18	0.39
$F(H\beta)$[e]	0.33	3.06	39.49	59.24	0.67	10.09
c[†]	0.88	—	0.17	—	1.06	—

TABLE 3

SOURCES OF PUBLISHED DATA

Reference	Type of Object
Dennefeld 1986	SNRs
Díaz et al. 1985	LINERs
Dinerstein & Shields 1986	H II regions
Ferland & Netzer 1983	LINERs
French 1980	H II regions
Heckman et al. 1980	LINERs
Keel 1983a	LINERs
Kirhakos & Phillips 1989	LINERs
Osterbrock 1989	Crab SNR
Osterbrock et al. 1992	Seyfert 2s
Stauffer 1982	LINERs, NELGs
Phillips et al. 1983	Seyfert 2s
Veilleux & Osterbrock 1987	Seyfert 2s, NELGs, and starbursts

AGNs to the 60–400 keV background (Rothschild et al. 1983) and was set to $\alpha = -2$. The actual spectral energy distribution of low-luminosity AGNs may be quite different from that of a single power law extending from infrared to X-ray energies. We adopted such a representation simply as a convenient means to alter the hardness of the ionizing continuum, which directly affects the average energy per photon. The calculations were terminated at a minimum temperature of 4000 K, below which it was verified that little optical emission is produced.

3.2. *Comparison with Observations*

We present our theoretical results in the form of several emission-line ratio diagnostic diagrams, in which we have plotted our new measurements along with additional data collected from several published sources (Table 3). In the optical region, we adopt the diagnostic diagrams of Veilleux & Osterbrock (1987) instead of those of Baldwin, Phillips, & Terlevich (1981). As Veilleux & Osterbrock (1987) have emphasized, the lines used in the line ratios should be as close as possible in wavelength so that errors due to reddening correction and relative flux calibration can be minimized. In the near-infrared region, we make use of the diagrams of Osterbrock, Tran, & Veilleux (1992) and Díaz, Pagel, & Wilson (1985; see also Kirhakos & Phillips 1989).

In all subsequent diagrams, the line intensities have been corrected for reddening as described in § 2.4. Filled circles correspond to objects whose emission-line ratios meet H80's criteria for LINERs; open circles denote objects which do not meet these criteria, but which have been classified as LINERs by other authors based on other criteria, most commonly by a high value of [N II] λ6583/Hα ($\gtrsim$0.6). We will call the latter group "transition objects," as we will argue that they are likely to be composite in nature. Our combined sample contains 47 low-excitation objects, of which 85% are LINERs and 15% are transition objects. Squares correspond to Seyfert 2 nuclei, Xs to H II regions, stars to starburst galaxies, five-pointed stars to supernova remnants (SNRs), and crosses to "narrow emission-line galaxies" (NELGs), which may be either AGNs or H II regions. The predicted line ratios are shown as various solid line segments, each labeled by the logarithm of (n/cm^{-3}).

The three Veilleux & Osterbrock (1987) diagrams, in which [O III] λ5007/Hβ is plotted against [N II] λ6583/Hα, [S II] λ6724/Hα, and [O I] λ6300/Hα, are shown in Figures 4–6. As discussed by Veilleux & Osterbrock, these diagrams are excellent discriminants of various classes of emission-line objects. H II regions and starburst galaxies tend to exhibit weak low-ionization lines relative to objects such as Seyfert 2 nuclei and LINERs, whose NLRs are heated by sources more energetic than young stars. They are well defined by the theoretical models of McCall, Rybski, & Shields (1985) for $T_{\rm eff}$ = 38,500–47,000 K, corresponding to oxygen abundances of O/H = 3.5–0.5 (O/H)$_\odot$. LINERs, on the other hand, are separated from Seyfert 2 nuclei (see Ho, Shields, & Filippenko 1993 for a discussion of their optical line intensity ratios) because they have lower excitation (lower values of [O III] λ5007/Hβ).

Examination of Figures 4–6 reveals that the LINERs are well segregated from the transition objects in that the former have much stronger low-ionization lines. The most striking difference is in the strength of [O I]/Hα, with LINERs having a ratio $\gtrsim\frac{1}{6}$; a similar trend is also observed in [S II]/Hα and [N II]/Hα. The strengths of the low-ionization lines of transition objects lie intermediate between those of low-metallicity H II regions and LINERs. We note that, after distinguishing objects which truly conform to H80's original classification criteria from those which do not, the *spread* of the observed values of the low-ionization lines in LINERs is reduced by $\sim$0.5 dex. The dichotomy in the strength of [O I]/Hα between LINERs and transition objects suggests that this ratio can be used to distinguish these two classes of emission-line objects in the event that incomplete wavelength coverage makes complete adherence to H80's criteria impractical.

Superposition of the predictions from our photoionization calculations on the Veilleux & Osterbrock diagrams indicates that the power-law models with a range in density ($n = 10^{2.5}$–$10^{5.5}$ cm^{-3}) and ionization parameter (log $U = -3$ to -4) can reasonably reproduce the range of observed low-ionization line ratios of LINERs (Figs 4–6; see Table 4 for a list of predicted and observed line ratios). The range of n which best brackets the observations depends on the given line. [N II] λ6583, for example, is suppressed for $n \gtrsim 10^5$ cm^{-3} because Lyα, [O III] λ5007, and Mg II λ2798 become dominant coolants under those conditions. [S II] λ6724, on the other hand, becomes very weak for $n \gtrsim 10^4$ cm^{-3} because of its low critical density ($\sim 10^3$ cm^{-3}). The calculations displayed assume $\alpha = -1.5$; modifying α to -1 and -2.5 changes [N II]/Hα by $\sim \pm 30\%$ and [O I]/Hα and [S II]/Hα by $\sim \pm 50\%$, with the higher values corresponding to the harder continuum. Taking these considerations into account, the observed spread of line

NOTES TO TABLE 2

[a] For each galaxy, the observed line intensity relative to Hβ is given in the first column; the second column shows the line intensity relative to Hβ after correction for internal reddening.

[b] [Ne III] λ3970 is blended with Hϵ.

[c] Contaminated by a broad Hα component.

[d] Value given is for the blended [S II] $\lambda\lambda$6716, 6731 doublet.

[e] Flux of the narrow component of Hβ in units of 10^{-14} ergs s^{-1} cm^{-2}.

[f] Reddening correction taken from Shields & Filippenko 1990.

[g] Assuming the [O III] λ4363/Hγ ratio of Filippenko & Sargent 1988.

[h] Reddening correction taken from Filippenko & Sargent 1988.

† Reddening correction factor $c \equiv E(B-V)/0.77$.

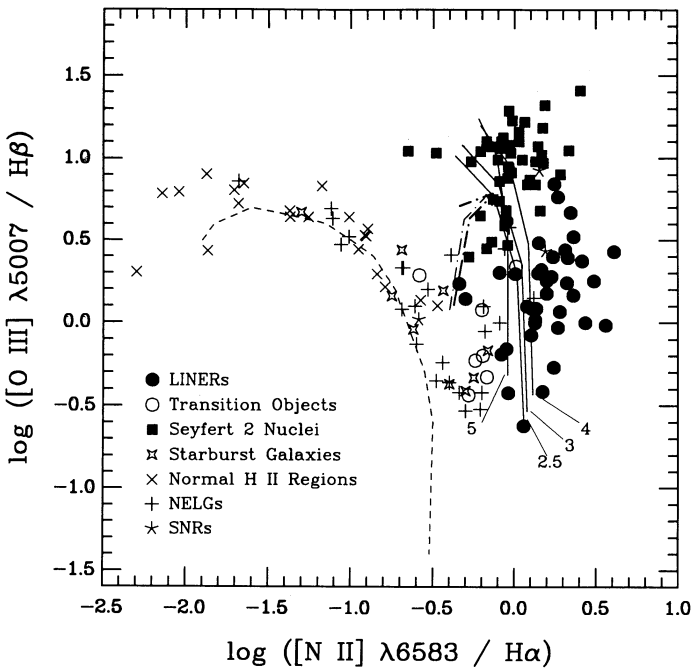

FIG. 4

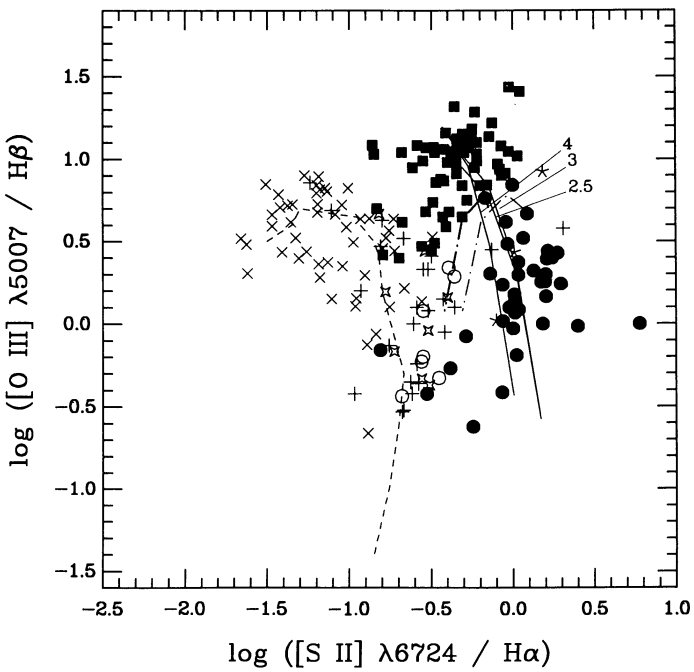

FIG. 5

FIG. 4.—Plot of log ([O III] λ5007/Hβ) vs. log ([N II] λ6583/Hα) (after Veilleux & Osterbrock 1987). Dashed line represents H II region track of McCall et al. (1985) for $T_* = 38{,}500$–$47{,}000$ K. All line fluxes have been corrected for internal reddening. Filled circles correspond to LINERs, open circles to transition objects (see text), squares to Seyfert 2 nuclei, Xs to H II regions, stars to starbursts, five-pointed stars to SNRs, and crosses to NELGs. Solid line segments denote power-law models with $\alpha = -1.5$ and solar abundances. Log U runs from -2.5 to -4 (*top to bottom*), and log $(n/\mathrm{cm}^{-3}) = 2.5$–5 are labeled for each line. The shock models of Raymond (1992) for $n_0 = 10\ \mathrm{cm}^{-3}$ (*light dot-dashed line*) and $100\ \mathrm{cm}^{-3}$ (*heavy dot-dashed line*) are shown for $v_s = 150\ \mathrm{km\ s}^{-1}$ (*top*) to $90\ \mathrm{km\ s}^{-1}$ (*bottom*).

FIG. 5.—Plot of log ([O III] λ5007/Hβ) vs. log ([S II] λ6724/Hα) (after Veilleux & Osterbrock 1987). Symbols same as in Fig. 4, except that only log $(n/\mathrm{cm}^{-3}) = 2.5$, 3, and 4 are shown.

ratios is well reproduced (Table 4), with the possible exception of [N II]/Hα. It appears that no reasonable combination of parameters is able to match the highest values of [N II]/Hα (~ 3) seen in Figure 4. Although taken at face value this might imply that objects with the highest [N II]/Hα ratios are preferentially enriched in N (e.g., Storchi-Bergmann & Pastoriza 1989, 1990; Storchi-Bergmann, Bica, & Pastoriza 1990; Cid-Fernandes et al. 1992), we caution that such a conclusion may be premature in light of the simplicity of the current single-density models. The data point on the far right of Figure 5 is NGC 2768 [log ([S II]/Hα) = 0.78]. Inspection of the spectrum shown in Heckman, Balick, & Crane (1980) indicates that the emission lines in this object are weak, so the line measurements may be very uncertain. The large spread of [S II]/Hα in Figure 5 probably reflects the sensitivity of the [S II] λ6724 doublet to collisional deexcitation.

Our power-law calculations are not able to match the observed line intensity ratios of the transition objects in a straightforward manner without invoking a highly contrived combination of model parameters. The simplest interpretation of their spectral characteristics is that both stellar and non-stellar processes contribute to the excitation of the ionized gas (see discussion in § 4.2).

The brightest lines in the near-infrared region observed in most emission-line galaxies are [O II] λ7325 and [S III] λλ9069, 9532. Osterbrock et al. (1992) used these, in conjunction with other bright optical lines, to define several useful diagnostic diagrams. Although the data are still very sparse, our study nearly doubles the sample of LINERs with available near-infrared line measurements. The ratio [O II] λ7325/Hα, in

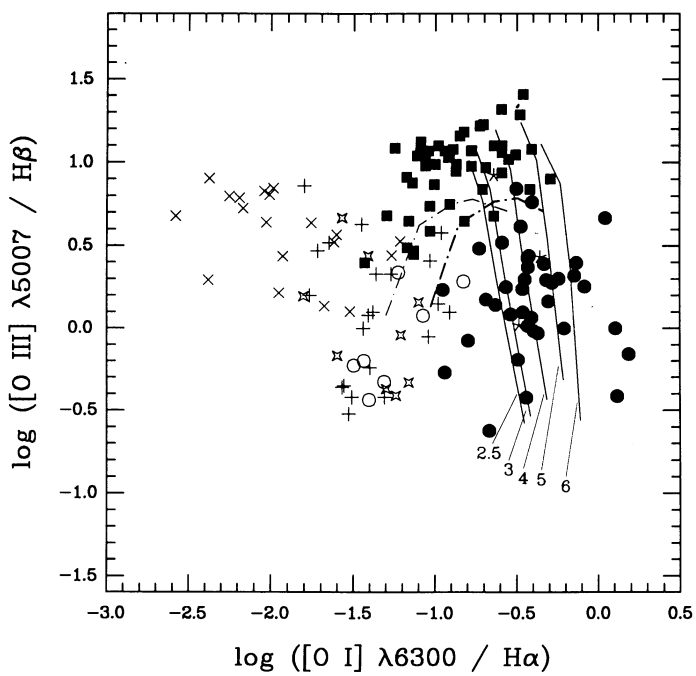

FIG. 6.—Plot of log ([O III] λ5007/Hβ) vs. log ([O I] λ6300/Hα) (after Veilleux & Osterbrock 1987). Symbols same as in Fig. 4, except that log $(n/\mathrm{cm}^{-3}) = 2.5$–6 are shown.

TABLE 4

PREDICTED AND OBSERVED LINE RATIOS IN LINERs[a]

Line Ratio (1)	log n = 2.5 (2)	log n = 3 (3)	log n = 4 (4)	log n = 5 (5)	Observed (6)
[O I] λ6300/Hα	0.07–0.61	0.08–0.67	0.10–0.87	0.13–1.28	0.16–1.60
[O I] λ6300/[O III] λ5007	0.32–0.67	0.29–0.68	0.26–0.76	0.23–0.95	0.1–6
[O II] λ3727/[O III] λ5007	4.90–3.46	4.26–3.09	2.05–1.60	0.39–0.35	0.45–25
[O II] λ7325/Hα	0.01–0.05	0.02–0.08	0.08–0.21	0.21–0.41	0.03–0.70
[O III] λ5007/Hβ	0.63–2.46	0.77–2.67	1.11–3.18	1.59–3.74	0.3–10
[N II] λ6583/Hα	0.66–1.45	0.73–1.51	0.84–1.62	0.58–1.36	0.9–3
[S II] λ6724/Hα	0.61–1.66	0.60–1.67	0.37–1.39	0.09–0.86	0.6–2.5
[S II] λ6724/[S III] λ9300[b]	1.93–1.85	1.74–1.77	0.88–1.30	0.22–0.74	1.1–22
[S III] λ9300[b]/Hα	0.32–0.89	0.35–0.95	0.42–1.07	0.45–1.15	0.05–0.9

[a] Predicted line ratios listed for log $U = -3.5$ and solar abundances. Col. (1) specifies the line ratio. Cols. (2)–(5) list the ratios for power-law models with different values of log (n/cm^{-3}); the range of values within each column correspond to varying α from -2.5 to -1. Col. (6) gives the range of observed values for LINERs.

[b] [S III] λ9300 designates the sum of [S III] λ9069 and [S III] λ9532.

addition to being a tool to separate different classes of emission-line objects when used in conjunction with the line intensity ratios [O III] λ5007/Hβ, [S III] λλ9069, 9532/Hα, and [S II] λ6724/Hα (see Figs. 7–9, as well as discussion in Osterbrock et al.), appears to be very sensitive to, and hence a useful indicator of, density over a wide range of values. The observed values of [O II] λ7325/Hα in LINERs, as well as in Seyfert 2 nuclei, show a very large spread (nearly a factor of 10); this spread, however, can be easily accounted for in our photoionization calculations by varying n from $10^{2.5}$ to 10^6 cm^{-3} for $\alpha = -1.5$. That a large range of n probably characterizes the line-emitting gas of the LINERs in our sample is supported by detailed profile analysis of the forbidden lines (§ 3.4). The sensitivity of [O II] λ7325 to n greatly overshadows the effect of varying the hardness of the ionizing continuum, although changing α can further contribute to the spread of [O II]/Hα (Table 4). The only transition object for which we have near-infrared data is NGC 3504; its position in Figures 7–9 coincides with those of H II regions.

As first pointed out by Díaz et al. (1985) and Kirhakos & Phillips (1989), photoionization models noticeably overestimate [S III] λλ9069, 9532. Figures 10 and 11, in which [S II]/Hα versus [S III]/Hα and [S II]/[S III] versus [O II] λ3727/[O III] are (respectively) plotted, illustrate that the data fall below the predictions by about a factor of 2. We have verified that no combination of U, n, or α appears capable of rectifying the discrepancy. A straightforward solution would be to selectively decrease the abundance of S by a factor of ~2 (Osterbrock et al. 1992); this acts to decrease the strength of [S III] relative to [S II], because, although both are reduced in strength, [S II] is reduced less because it is a more important coolant than [S III]. But, as cautioned by Osterbrock et al. (1992), the simplicity of

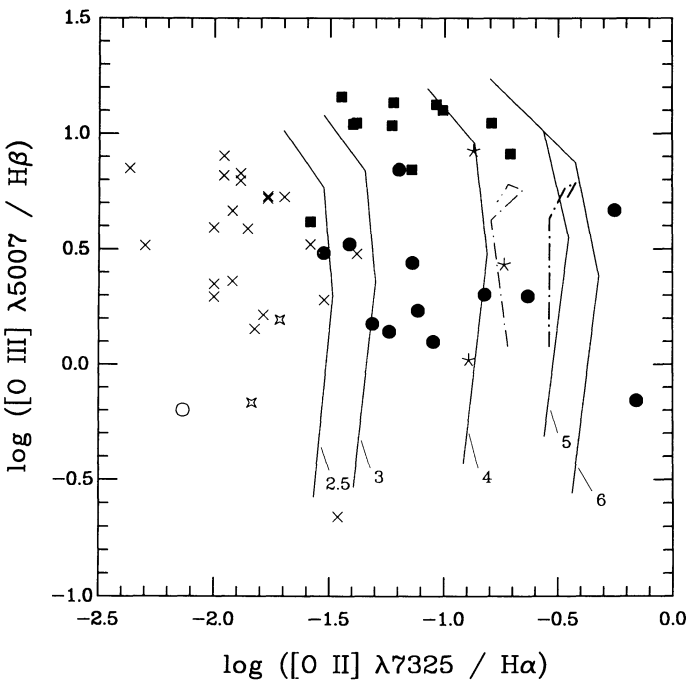

FIG. 7

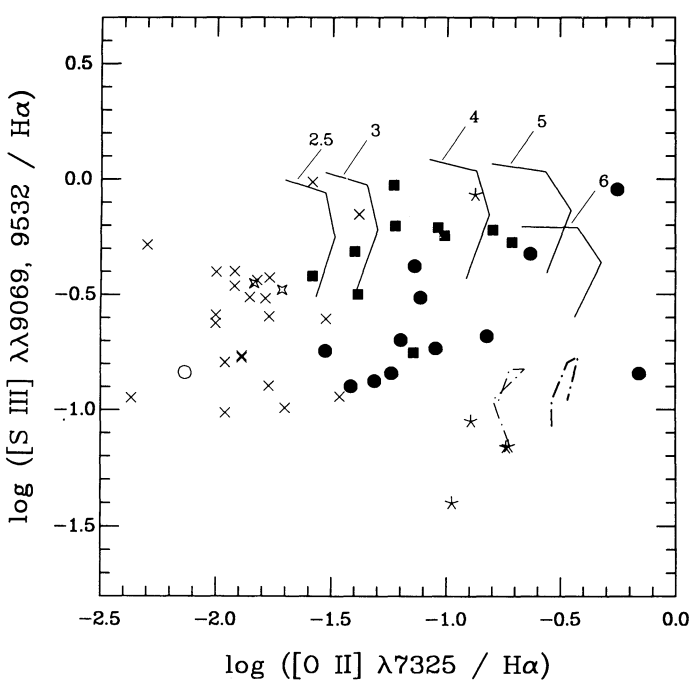

FIG. 8

FIG. 7.—Plot of log ([O III] λ5007/Hβ) vs. log ([O II] λ7325/Hα) (after Osterbrock et al. 1992). Symbols same as in Fig. 4, except that log (n/cm^{-3}) = 2.5–6 are shown.

FIG. 8.—Plot of log ([S III] λλ9069, 9532/Hα) vs. log ([O II] λ7325/Hα) (after Osterbrock et al. 1992). Symbols same as in Fig. 4, except that log (n/cm^{-3}) = 2.5–6 are shown. For the shock models, the shock velocities increase from 90 km s^{-1} (*bottom*) to 150 km s^{-1} (*top*).

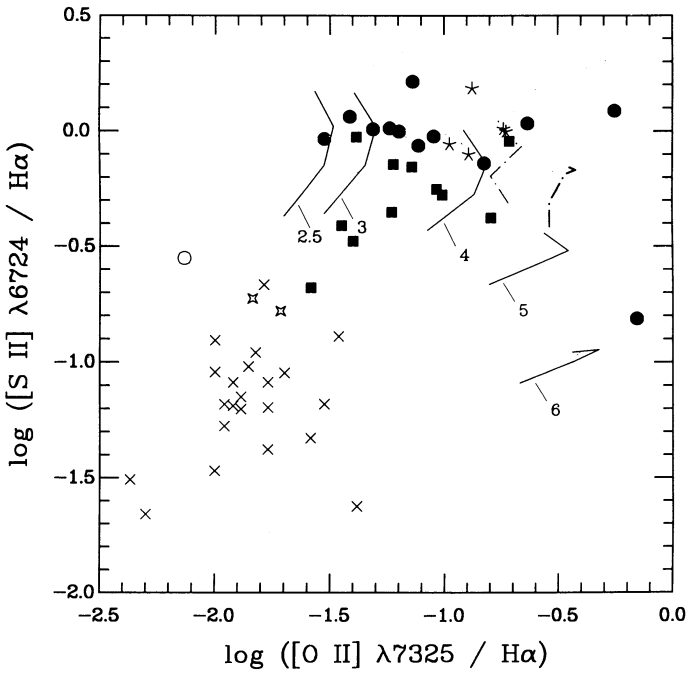

FIG. 9

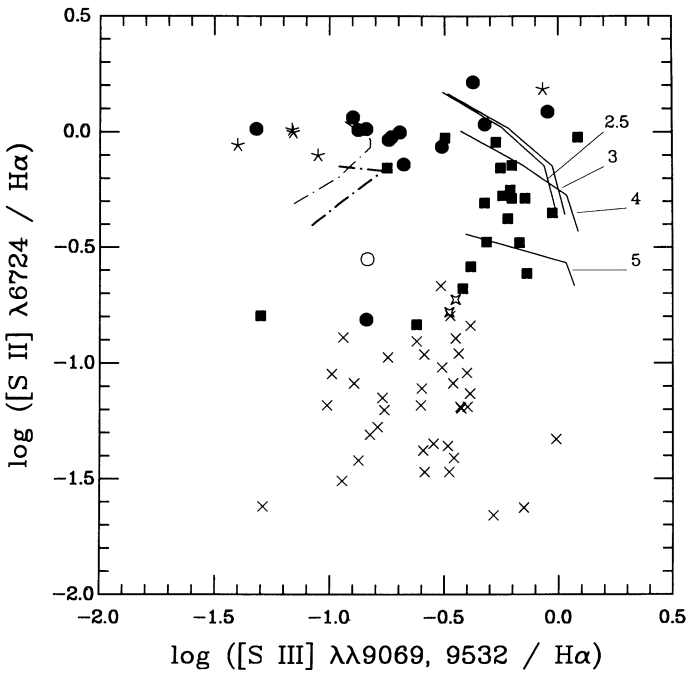

FIG. 10

FIG. 9.—Plot of log ([S II] λ6724/Hα) vs. log ([O II] λ7325/Hα) (after Osterbrock et al. 1992). Symbols same as in Fig. 4, except that log (n/cm^{-3}) = 2.5–6 are shown.

FIG. 10.—Plot of log ([S II] λ6724/Hα) vs. log ([S III] λλ9069, 9532/Hα) (after Díaz et al. 1985). Symbols same as in Fig. 4, except that log (n/cm^{-3}) = 2.5–5 are shown. Log U varies from −2.5 (*right*) to −4 (*left*). The shock velocities increase from 90 km s^{-1} (*left*) to 150 km s^{-1} (*right*).

current photoionization models does not justify such inferences concerning the abundances of the line-emitting gas. Osterbrock et al. (1992) postulate that perhaps a combination of matter-bounded clouds and an additional heating source from relativistic electrons (e.g., Viegas-Aldrovandi & Gruenwald 1988) may provide a solution. Moreover, it is conceivable that part of the discrepancy may be due to errors in atomic data. The collision strength of S^{++} used in CLOUDY appears to be fairly reliable (Pradhan & Gallagher 1992), but it is possible that the total recombination rate is uncertain (Pradhan 1993).

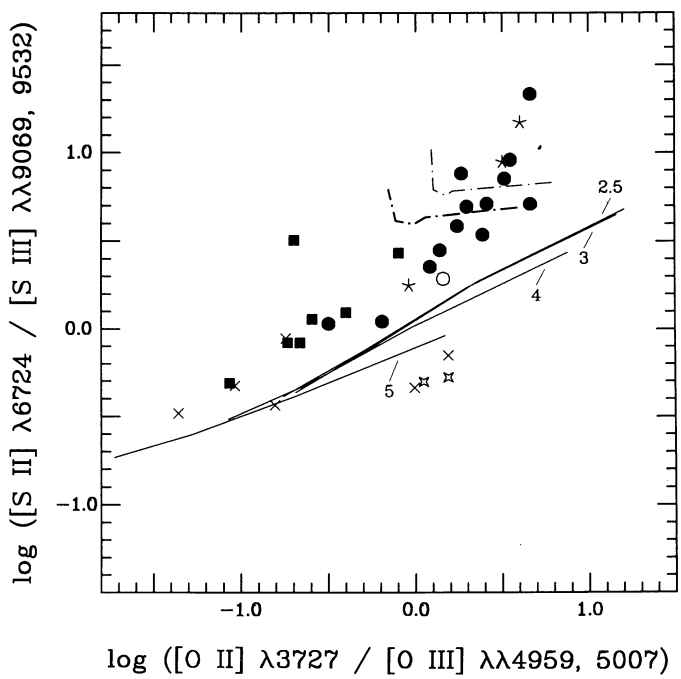

FIG. 11.—Plot of log ([S II] λ6724/[S III] λλ9069, 9532) vs. log ([O II] λ3727/[O III] λλ4959, 5007) (after Díaz et al. 1985). Symbols same as in Fig. 4, except that log (n/cm^{-3}) = 2.5–5. Log U varies from −2.5 (*left*) to −4 (*right*). The shock velocities increase from 90 km s^{-1} (*right*) to 150 km s^{-1} (*left*).

3.3. *Comparison with Shock Calculations*

In Figures 4–11, plane-parallel shock calculations (Raymond 1992) assuming solar abundances, equilibrium preionization, and shock velocities v_s = 90, 100, 110, 130, and 150 km s^{-1} are shown for a preshock density of n_0 = 10 cm^{-3} (*light dot-dashed line*) and 100 cm^{-3} (*heavy dot-dashed line*). These shock models were preferred over the widely used ones of Shull & McKee (1979) because they incorporate updated atomic parameters. Although shock models match the [S III]/Hα and [S II]/[S III] ratios of some LINERs (Figs. 10 and 11), they appear to fall considerably short of reproducing the other line intensity ratios for a majority of LINERs. For the range of shock velocities and preshock densities chosen, [O III]/Hβ is too strong while [O I]/Hα, [S II]/Hα, and [N II]/Hα are too weak compared with observations (Figs. 4–6). The range of [O II]/Hα produced by the shock models, although overlapping with the values of some LINERs, seems too narrow to encompass most of the data (Figs. 7–9). Part of the discrepancy might be due to the small range of parameter space covered by the present calculations; shock models incorporating higher preshock densities should be compared with the observations. It is especially disturbing that shock models only account for some, but not all, of the line intensity ratios of supernova remnants (SNRs), objects which *should* be excited by shocks. Either the shock models are incomplete or SNRs are more complex than we thought.

3.4. *Evidence for Density Stratification*

The photoionization calculations described in § 3.2 suggest that the large range of [O II] λ7325/Hα ratios observed in LINERs may reflect that some objects have large densities in their NLR. Filippenko & Sargent (1988, and references therein) have shown that the existence of a line width versus critical density correlation for the forbidden lines of a few well-studied LINERs, a phenomenon also seen in Seyfert 2 nuclei (De Robertis & Osterbrock 1986), implies that a range of densities is present in the NLRs of these objects. In particular, densities up to four orders of magnitude higher than that conventionally derived from the [S II] λλ6716, 6731 doublet ($n_e \approx 10^3$ cm^{-3}) have been inferred from other forbidden lines.

We applied the analysis of Filippenko & Sargent (1988) to the objects in our sample for which we could measure the FWHM of the prominent forbidden lines. As discussed in § 2.2, spectra with higher spectral resolution were used to separate [N II] λλ6548, 6583 from Hα and to deblend [S II] λ6716, 6731. The majority (nine out of 12, or 75%) of the LINERs in our sample exhibit a line width versus critical density correlation; the only three which do not are NGC 1167, NGC 2639, and NGC 7479. By contrast, the transition object NGC 3504 failed to show such a correlation. It is perhaps significant that the three LINERs which do *not* show the correlation have substantially weaker [O II] λ7325/Hα (⟨[O II]/Hα⟩ = 0.04) compared to the rest of the sample (⟨[O II]/Hα⟩ = 0.12). NGC 7213 has the highest value of [O II]/Hα (∼0.69) in our combined sample; Filippenko & Halpern (1984) showed that it exhibits a prominent line width versus critical density correlation. This result suggests that LINERs with large [O II]/Hα ratios are more likely to have high densities in their NLR, as presaged by the photoionization calculations (§ 3.2). We emphasize that a much larger sample is needed to confirm this finding.

4. EXCITATION MECHANISMS

4.1. *Photoionization by a Nonstellar Continuum*

We have demonstrated that the main optical to near-infrared spectral features of LINERs, with the possible exception of [S III] λλ9069, 9532, are well modeled with photoionization by a nonstellar ionizing continuum. The very large spread of several line intensity ratios (e.g., [N II]/Hα and [S II]/Hα), previously attributed to selective enrichment, for example, is (1) substantially reduced by distinguishing between "true" LINERs and transition objects, and (2) better reproduced by varying input parameters in the photoionization models such as the density and the hardness of the ionizing continuum. The discrepancy between the predicted and observed values of the near-infrared [S III] lines might be rectified with improved atomic data.

Suggestions have often been made (e.g., Péquignot 1984; Viegas-Aldrovandi & Gruenwald 1990) that a power law is a poor representation of the shape of the ionizing continuum for LINERs, and that a $\sim 10^5$ blackbody with an extended X-ray tail yields better agreement with several weaker spectral features. In particular, such blackbody models yield smaller values for the He II λ4686/Hβ ratio, in better agreement with observations than the predictions from the power-law models of Ferland & Netzer (1983). While we fully recognize that a single power law is probably a vast oversimplification of the shape of the actual ionizing continuum source, our present calculations indicate that for log $U = -3.5$ and $\alpha = -1$ to -2, He II/Hβ ≈ 0.05–0.12 (the results are independent of density for $n = 10^{2.5}$–10^6 cm^{-3}), in excellent agreement with the observed range of ∼0.06–0.16, especially taking into consideration the large uncertainties associated with the measurement of the weak He II λ4686 line. Contrary to the blackbody models of Viegas-Aldrovandi & Gruenwald (1990), our calculations also satisfactorily predict the observed range of values of [N I] λ5200/[N II] λλ6548, 6583 (0.02–0.1); we thus find it unnecessary to appeal to matter-bounded clouds for most LINERs, although they cannot be eliminated for some LINERs which have much stronger [N I]/[N II] (Viegas-Aldrovandi & Gruenwald 1988). Both power laws and blackbodies yield a fairly narrow range of values for He I λ5876/Hβ (∼0.15) for a wide range of initial conditions. Although this appears to be incompatible with some of the observed values which may be a factor of 2–3 lower, the He I λ5876 line may be subject to large uncertainties because of its proximity to the interstellar Na D λ5893 absorption feature. High spectral resolution observations would help to clarify the situation.

Finally, the large strength of the [O III] λ4363 line observed in LINERs has often been cited as supporting evidence for an additional heating mechanism such as shocks or relativistic electrons associated with a nuclear radio source (Cesar, Aldrovandi, & Gruenwald 1985; Viegas-Aldrovandi & Gruenwald 1988, 1990). But, as noted by Filippenko & Halpern (1984) and Filippenko (1985), the presence of high-density gas in the NLR will enhance $R \equiv$ [O III] λ4363/[O III] λλ4959, 5007, thus leading to an overestimate of the electron temperature. Our calculations support this conclusion. For log $U = -3.5$, $\alpha = -1.5$, and $n = 10^6$ and 10^7 cm^{-3}, $R = 0.03$ and 0.27, respectively, in good agreement with the observed range of 0.02–0.13. Moreover, many of the LINERs in our sample show evidence for high densities (§ 3.4).

Broad Hα emission is clearly present in several of the LINERs in our combined sample; our sample alone contains four (NGC 315, 1167, 3031, and 3998), and possibly eight (including NGC 1052, 2639, 3642, and 7479) candidates. By analogy with Seyfert 1 nuclei, the presence of broad Hα emission suggests that at least these LINERs might be photoionized by a nonstellar continuum source, such as that generated by accretion onto a massive compact object. A realistic estimate of the fraction of LINERs which harbor broad Hα emission must await full analysis of the Palomar survey, but the preliminary results of Filippenko & Sargent (1985) indicate that this fraction may be as high as ∼30%.

Although the purported nonstellar ionizing continuum of LINERs has not yet been convincingly detected either in the optical or the ultraviolet spectral region, recent BBXRT observations (Mushotzky 1993) have detected pointlike X-ray emission in several bright LINERs (including NGC 3031 and NGC 3998). These results strengthen the apparent continuity between LINERs and Seyfert 1 nuclei, even if the detailed X-ray properties differ between them (Mushotzky 1993). Additional similarities between LINERs and "classical AGNs" are suggested by the frequency of the detection of compact radio cores (e.g., H80), as well as the presence of a radio jet in NGC 315 (Giovannini, Feretti, & Comoretto 1989).

4.2. *The Nature of the Transition Objects*

We have found that the incomplete, heterogeneous sample assembled for this study contains a small fraction (∼15%) of objects which have been previously misclassified as LINERs.

The properties of the optical–to–near-infrared emission-line spectra of these "transition objects" appear to be intermediate between those of H II regions and LINERs; their low-ionization lines are stronger than those of the former, yet weaker than those of the latter. Relative to LINERs as a class, they invariably show [O I]/H$\alpha \lesssim \frac{1}{6}$, thus motivating Filippenko & Terlevich (1992) and Ho & Filippenko (1993) to coin the name "weak–[O I] LINERs." The simplest explanation of the observed line intensity ratios of the transition objects is that they are composite H II region/LINER systems—that is, either nebulae which are excited *both* by hot stars and by nonstellar radiation, or *mixtures* of normal H II regions and nebulae excited by nonstellar radiation.

Close inspection of the transition objects indeed confirms our hypothesis. NGC 3504, from our own data sample, shows prominent Balmer absorption lines superposed on a very blue continuum (Fig. 1*d*). Moreover, Kenney et al. (1992) detect a large concentration of molecular gas in the nucleus of NGC 3504, suggesting that an inflow of gas might have triggered a nuclear starburst. Similarly, signatures of young stars are apparent in the optical spectra of Mrk 298 (Véron-Cetty & Véron 1984), NGC 6764 (Koski 1978), and Kaz 26 (Shuder 1981). Conti (1991) further notes that NGC 6764 shows evidence for broad He II λ4686, a distinctive feature of Wolf-Rayet stars. One of the transition objects is the narrow-line radio galaxy 3C 178; in addition to its unusually low ionization state, Balmer absorption lines are present in its optical spectrum (Costero & Osterbrock 1977). Finally, the very high far-infrared luminosity of NGC 4569 (Neff & Hutchings 1992) suggests that it is currently undergoing vigorous star formation.

Alternatively, it is possible to model the optical spectral properties of the transition objects ("weak–[O I] LINERs") with photoionization by very hot O-type stars alone. Filippenko & Terlevich (1992) demonstrate that a nebula irradiated by the continuum of O stars with $T_{\rm eff} = 45{,}000$ K (type O4 or earlier) is sufficient to generate the requisite spectral features of these objects if the gas is assumed to be metal rich (relative to normal H II regions) and if the ionization parameter is unusually low ($\log U \approx -3.5$). Filippenko & Terlevich argue that although O stars with such high effective temperatures do not follow the apparent inverse correlation between $T_{\rm eff}$ and metallicity observed in normal H II regions (e.g., McCall et al. 1985), they might be formed in the environment of early-type galactic nuclei. This combination of conditions cannot be excluded with current observational evidence, but we believe that the hypothesis that transition objects are composite H II region/LINER systems is more plausible, especially in light of the evidence for the presence of current star formation mentioned above. This hypothesis can be tested observationally by conducting a careful search for X-ray point sources, compact nuclear radio sources, or broad Hα emission in a large sample of transition objects.

We emphasize that the mere presence of young stars in the nucleus is generally *not* a sufficient condition for an emission-line galaxy to be classified as a transiton object. Both Mrk 700 (Koski 1978) and NGC 404, and to a lesser extent NGC 7743, have prominent Balmer absorption lines in their spectra, indicating the presence of a substantial population of A-type stars. Yet, they fully satisfy the H80 classification criteria of a LINER. It appears that the important factor is the relative strength of the LINER component compared to that of the young stars.

4.3. *LINERs as Stellar Phenomena*

In recent years, it has been recognized that the narrow-line emission spectrum of objects such as Seyfert nuclei and LINERs need not necessarily be attributed to nonstellar phenomena. Terlevich & Melnick (1985) showed that an ionizing continuum resembling a power law with $\alpha \approx -1.5$ can be produced by a cluster of Wolf-Rayet stars in the high-metallicity environment of galactic nuclei. In this scenario, the interaction of supernova remnants with dense circumstellar gas (Terlevich et al. 1992) can account for the broad Hα seen in some LINERs, although a recent study of the low-luminosity Seyfert 1 nucleus in NGC 4395 poses a serious challenge to the theory (Filippenko, Ho, & Sargent 1993).

Shields (1992) argues that many, or even most, LINERs may owe their excitation mechanism to very hot O-type stars; to account for the broad range of observed line ratios, the NLR is assumed to have several components with a wide range of densities and ionization parameters. In this picture, the NLR of LINERs with small ratios of low-ionization to recombination lines is characterized by values of U which are considered "typical" of LINERs ($\sim 10^{-3}$ to 10^{-4}; e.g., Ferland & Netzer 1983), and fairly low densities ($n \approx 10^3$ cm^{-3}). In order to account for objects with low-ionization lines which lie on the upper end of the observed dispersion, the NLR is assumed to have a component with an ionization parameter nearly two orders of magnitude lower than the canonical range. To produce the largest observed values of [O I] λ6300/Hα, for example, U has to be as low as $\sim 10^{-5.5}$ to 10^{-6}, which is achieved by increasing n to $\sim 10^{5.5}$–10^6 cm^{-3} if both the radiation field and the distance between the ionizing continuum source and the irradiated NLR are fixed. Such small values of U appear to be in conflict with the [O III]/Hβ ratios observed in these objects (see Fig. 6), since [O III]/Hβ decreases as U decreases, unless it is assumed that the O^{++} zone has a *higher* value of U (and hence *lower* n) than the O^0 zone. The presence of a line width versus critical density correlation in many LINERs argues against this possibility.

4.4. *Evidence for Shock Heating*

Shock heating can give rise to a LINER-like emission-line spectrum in a variety of astrophysical settings such as cooling flows, starburst-driven winds, and galaxy interactions (see, e.g., Filippenko 1993). The emission in these systems, however, is generally extended ($r \lesssim 2$ kpc). The existence of shock heating in galactic *nuclei* ($r \lesssim 200$ pc), on the other hand, remains at present unknown. In a recent study of infrared line diagnostics of AGNs, Spinoglio & Malkan (1992) suggest that the mid-infrared line ratios [Ne III] 15.6 μm/[Ar II] 7 μm and [Ne III] 15.6 μm/[Ne II] 12.8 μm tend to be much weaker in shocks relative to photoionized gas, and, as such, may serve as useful shock signatures. These conclusions, however, were based on the models of Binette, Dopita, & Tuohy (1985) for fast shocks (v_s up to 1080 km s^{-1}); their application to galactic nuclei having much lower velocity dispersions appears questionable. Current plane-parallel shock calculations assuming more reasonable shock velocities are difficult to evaluate in the optical to near-infrared region (§ 3.3), although calculations incorporating higher densities may account for part of the discrepancy between the model predictions and observations. Genuine progress may have to await construction of more sophisticated models and availability of more accurate atomic data.

4.5. *Future Directions*

This study demonstrates that analysis of the excitation mechanism of weak emission-line objects such as LINERs requires spectra of high-quality covering a wide wavelength range. Accurate line measurements can be made only after careful removal of the underlying starlight from the observed spectra. Although we find that our method of template subtraction works reasonably well for most objects with an old stellar population in the bulge, more sophisticated techniques need to be implemented to treat those nuclei which contain younger stars. This effort must be applied to a large, statistically complete sample of objects observed in a uniform manner. Such an analysis is currently in progress for the Filippenko & Sargent (1985) survey of ~ 500 galaxies.

On the theoretical front, more sophisticated shock and photoionization calculations need to be performed. In particular, a realistic density structure of the NLR needs to be incorporated into the models, reflecting the mounting evidence that a range of densities is present. Lastly, the theoretical uncertainty of the near-infrared [S III] lines needs to be addressed.

5. CONCLUSIONS

We have analyzed a large sample of LINERs with high-quality spectra covering a wide wavelength region. Careful attention has been paid to removing the underlying starlight contamination, allowing accurate determination of line fluxes. We used these measurements along with relevant published data to examine the excitation mechanisms of LINERs with compact ($r \lesssim 200$ pc) emission-line gas. Theoretical line ratios for collisional excitation by shocks as well as photoionization by stellar and nonstellar continua were compared with the observations. Our findings can be summarized as follows:

1. The overall optical to near-infrared spectral features of LINERs are adequately reproduced by photoionization calculations which assume a nonstellar ionizing continuum, solar abundances, and ionization parameters in the range $\sim 10^{-3}$ to 10^{-4}. Allowance for variations in the total hydrogen density and in the hardness of the ionizing continuum accounts for the range of observed line intensity ratios in the optical and near-infrared diagnostic diagrams. The detection of weak, broad Hα emission and pointlike X-ray sources in several of these objects supports the hypothesis that they are low-luminosity AGNs.

2. We find that many of the LINERs in our sample show evidence for density stratification in the NLR. The [O II] λ7325/Hα ratio appears to be very sensitive to variations in density and, as such, can be used as a crude density indicator for the NLR.

3. The importance of shock excitation for LINERs in galactic nuclei is difficult to assess with the present plane-parallel shock models. The predicted line intensity ratios differ systematically from observations in the optical region, possibly because the range of parameter space (e.g., preshock densities) explored thus far is too narrow.

4. Approximately 15% of all objects previously classified as LINERs appear to be composite H II region/LINER sytems experiencing ongoing nuclear or circumnuclear star formation.

We acknowledge the financial support of NSF grant AST-8957063 and NASA grant NAG 5-1800 to A. V. F., and by NSF grant AST-891971 to W. L. W. S. Support for this work was also provided by NASA through grant GO-3507.01-91A from the Space Telescope Science Institute, which is operated by the Association of Universities for Research in Astronomy, Inc., under NASA contract NAS 5-26555. We thank W. C. Keel for his informative referee report and J. C. Shields for providing detailed comments and suggestions which led to substantial improvements in this paper. We are very grateful to G. Ferland for generously making available his code CLOUDY and to J. Raymond for providing us with the shock calculations shown in § 3.3. Assistance with the observations at Palomar Observatory (Juan Carrasco, Mike Doyle, and John Henning) and at Lick Observatory (Barry Alcott, Jim Burrows, and John Morey) is appreciated. W. L. W. S. thanks the Miller Institute for Basic Research in Science (U. C. Berkeley) for a Visiting Miller Research Professorship during the completion of this paper.

REFERENCES

Baldwin, J. A., Phillips, M. M., & Terlevich, R. 1981, PASP, 93, 5
Bica, E. 1988, A&A, 195, 76
Binette, L., Dopita, M. A., & Tuohy, I. R. 1985, ApJ, 297, 476
Brocklehurst, M. 1971, MNRAS, 153, 471
Burstein, D., & Heiles, C. 1984, ApJS, 54, 33
Cardelli, J. A., Clayton, G. C., & Mathis, J. S. 1989, ApJ, 345, 245
Cesar, M. L., Aldrovandi, S. M. V., & Gruenwald, R. B. 1985, PASP, 97, 850
Cid Fernandes, R., Jr., Dottori, H. A., Gruenwald, R. B., & Viegas, S. M. 1992, MNRAS, 225, 165
Conti, P. S. 1991, ApJ, 377, 115
Costero, R., & Osterbrock, D. E. 1977, ApJ, 211, 675
Dennefeld, M. 1986, A&A, 157, 267
De Robertis, M. M., & Osterbrock, D. E. 1986, ApJ, 301, 727
Díaz, A. I., Pagel, B. E. J., & Wilson, I. R. G. 1985, MNRAS, 212, 737
Dinerstein, H. L., & Shields, G. A. 1986, ApJ, 311, 45
Ferland, G. J. 1991, Ohio State University Internal Report 91-01 (Columbus: OSU Astronomy)
———. 1993, in The Nearest Active Galaxies, ed. J. Beckman (Madrid: CSIC), in press
Ferland, G. J., & Netzer, H. 1983, ApJ, 264, 105
Filippenko, A. V. 1982, PASP, 94, 715
———. 1985, ApJ, 289, 475
———. 1993, in The Nearest Active Galaxies, ed. J. Beckman (Madrid: CSIC), in press
Filippenko, A. V., & Halpern, J. P. 1984, ApJ, 285, 458
Filippenko, A. V., Ho, L. C., & Sargent, W. L. W. 1993, ApJ, 410, L75
Filippenko, A. V., & Sargent, W. L. W. 1985, ApJS, 57, 503
———. 1988, ApJ, 324, 134
Filippenko, A. V., & Terlevich, R. 1992, ApJ, 397, L79
Fosbury, R. A. E., Melbold, U., Goss, W. M., & Dopita, M. A. 1978, MNRAS, 183, 549
French, H. B. 1980, ApJ, 240, 41
Giovannini, G., Feretti, L., & Comoretto, G. 1989, ApJ, 358, 159
Grevesse, N., & Anders, E. 1989, in Cosmic Abundances of Matter, ed. C. J. Washington (New York: AIP), 1
Halpern, J. P., & Steiner, J. E. 1983, ApJ, 269, L137
Heckman, T. M. 1980, A&A, 87, 152 (H80)
Heckman, T. M., Balick, B., & Crane, P. C. 1980, A&AS, 40, 295
Ho, L. C., & Filippenko, A. V. 1993, Ap&SS, in press
Ho, L. C., Shields, J. C., & Filippenko, A. V. 1993, ApJ, 410, 567
Keel, W. C. 1983a, ApJ, 269, 466
———. 1983b, ApJS, 52, 229
Kenney, J. D. P., Wilson, C. D., Scoville, N. Z., Devereux, N. A., & Young, J. S. 1992, ApJ, 395, 79
Kirhakos, S., & Phillips, M. M. 1989, PASP, 101, 949
Koski, A. T. 1978, ApJ, 223, 56
Lawrence, A., & Elvis, M. 1982, ApJ, 256, 410
Leitherer, C., Gruenwald, R., & Schmutz, W. 1992, in Physics of Nearby Galaxies, ed. T. X. Thuan, C. Balkowski, & J. T. T. Van (Paris: Editions Frontières), in press
Massey, P., Strobel, K., Barnes, J. V., & Anderson, E. 1988, ApJ, 328, 315
McCall, M. L., Rybski, P. M., & Shields, G. A. 1985, ApJS, 57, 1
Mushotzky, R. F. 1993, in The Nearest Active Galaxies, ed. J. Beckman (Madrid: CSIC), in press
Neff, S. G., & Hutchings, J. B. 1992, AJ, 103, 1746
Oke, J. B., & Gunn, J. E. 1982, PASP, 94, 586

Oke, J. B., & Gunn, J. E. 1983, ApJ, 266, 713
Osterbrock, D. E. 1989, Astrophysics of Gaseous Nebulae and Active Galactic Nuclei (Mill Valley: University Science Books)
Osterbrock, D. E., Tran, H. D., & Veilleux, S. 1992, ApJ, 389, 196
Péquignot, D. 1984, A&A, 131, 159
Phillips, M. M., Charles, P. A., & Baldwin, J. A. 1983, ApJ, 266, 485
Phillips, M. M., Jenkins, C. R., Dopita, M. A., Sadler, E. M., & Binette, L. 1986, AJ, 91, 1062
Pradhan, A. K. 1993, private communications
Pradhan, A. K., & Gallagher, J. W. 1992, Atomic Data Nucl. Data Tables, 52, 227
Raymond, J. 1992, private communications
Rees, M. J. 1984, ARA&A, 22, 471
Rothschild, R., Mushotzky, R. F., Baity, W., Gruber, D., Matteson, J., & Peterson, L. 1983, ApJ, 269, 423
Schachter, J. 1991, PASP, 103, 457
Shields, J. C. 1992, ApJ, 399, L27
Shields, J. C., & Filippenko, A. V. 1990, ApJ, 353, L7
Shuder, J. M. 1981, ApJ, 244, 12
Shull, J. M., & McKee, C. F. 1979, ApJ, 227, 131
Silva, D. A. 1991, Ph.D. thesis, Univ. of Michigan
Spinoglio, L., & Malkan, M. A. 1992, ApJ, 399, 504
Stauffer, J. R. 1982, ApJ, 262, 66
Storchi-Bergmann, T., Bica, E., & Pastoriza, M. G. 1990, MNRAS, 245, 749
Storchi-Bergmann, T., & Pastoriza, M. G. 1989, ApJ, 347, 195
———. 1990, PASP, 102, 1359
Terlevich, R., & Melnick, J. 1985, MNRAS, 213, 841
Terlevich, R., Tenorio-Tagle, G., Franco, J., & Melnick, J. 1992, MNRAS, 255, 713
Veilleux, S., & Osterbrock, D. E. 1987, ApJS, 63, 295
Véron-Cetty, M.-P., & Véron, P. 1984, A Catalog of Quasars and Active Nuclei, ESO Scientific Rep. No. 1
———. 1986, A&AS, 66, 335
Viegas-Aldrovandi, S. M., & Gruenwald, R. B. 1988, ApJ, 324, 683
———. 1990, ApJ, 360, 474
Weedman, D. W. 1977, ARA&A, 15, 69